1   Dear Editor,

2   please find below the answers to the remarks of the reviewer. We want to thank to the
3   reviewer for his/her constructive comments.

4   Our replies are highlighted with red font and ** symbols.

5   The authors

6

7   General comments

8   Compared to its first submitted version, the paper by Mateos et al. has largely improved. Now I
9   find the discussion in Appendix A and Section 4 more consistent and complete. The reader has
10   now all the elements to evaluate the accuracy of the results. The paper benefits of this.
11   However I have to say that I find the discussion of the trends still quite weak and, in my point
12   of view, difficult to trust. Personally, by looking at Figure 4 I am not at all persuaded that there
13   is a real trend in the data (despite the results of your statistical analysis suggest this). I observe
14   a large variability in the AOD, which however can be linked to the different conditions and data
15   availability at the various sites, as well as "climate" parameters, such as the QBO, as also
16   discussed in the text. So, I suggest the authors not to stress too much this part in the paper (I
17   would reconsider point 2 in the conclusions, for instance). I would suggest analysing the results
18   of the AOD, ARE and forcing efficiency mostly with the point of view of a "multi-year dataset",
19   so discussing the spatial and interannual variability. As stated by the authors, in fact, this work
20   analyses an extended dataset and provides a large view of the Iberian Peninsula, so I think the
21   authors should concentrate mostly on this aspect. I would avoid looking at these data as a
22   database for trend analysis over the Penisula.

23   Based on this, I would encourage the authors to adapt the discussion accordingly.

24   ** Following the reviewer's suggestion, we stress the main results of the paper, not focusing
25   on the temporal trends. Hence, in the new version of the manuscript:

26   -   Temporal trends are not mentioned in the abstract.
27   -   The large variability of the annual means of Figure 4 is more clearly stated. We only
28   maintain the results for Barcelona site (which are statistically significant). In spite of
29   the large variability, it is evident that a slight decrease in the AOD levels occurs in the
30   Iberian Peninsula. Hence, the discussion of the causes behind this behavior, also based
31   on previous studies, is required to well understand the aerosol evolution in the 2000s.
32   -   The discussion of the trends shown in Figure 5 was removed.
33   -   Looking at Figure 6 (mean series between 2004 and 2012), we have decided to
34   maintain the discussion of the trends. In spite of the annual variability, the trend rates
35   are clearer in this figure.
36   -   The conclusion#2 of the previous manuscript was removed. In the new version, the
37   trend rates are only mentioned as a sentence to link the ARE and AOD evolution.

38

39   Specific comments

40   Lines 65-66: please rewrite or split in two sentences.

41   ** Modified: "Aerosol radiative effects in the LW range (ARE_{LW}) for dust particles are expected

42   to be smaller than in the SW"

43   Lines 514-516: I do not understand what you mean, please rewrite.

44   ** Rephrased. "The experimental retrievals of SSA and g for these cases with low AOD present

45   large uncertainties, and no reliable information can be used to verify our assumption."

46   Figure 4: please gives an indication of a scale for the symbols (a big symbol corresponds to

47   more than 100 cases? 200 cases?)

48   ** "Figure 4.   …Larger the symbols, large amount of data number that year (e.g., the smallest

49   symbols indicate cases between 100 and 150 points, while the largest symbols show years with

50   >250 points)."

51   Figure A1: it is not clear how to read the Figure, please clarify this in the caption:

52   ** "Figure A1. Dependence on aerosol load of the error committed when the optical

53   properties are fixed in the different spectral ranges for two SZAs (30º solid lines and symbols,

54   and 60º dashed lines and open symbols), and continental clean (CC, a) and continental

55   polluted (CP, b) aerosols."

1 Aerosol radiative effects in the ultraviolet, visible, and near-infrared spectral ranges using long-term

2 aerosol data series over the Iberian Peninsula

3

4 D. Mateos[1,2], M. Antón[1], C. Toledano[2], V. E. Cachorro[2], L. Alados-Arboledas[3,4], M. Sorribas[3,4,5],

5 M.J. Costa[6], J.M. Baldasano[7].

6 1. Departamento de Física, Universidad de Extremadura, Badajoz, Spain

7 2. Grupo de Óptica Atmosférica, Universidad de Valladolid, Valladolid, Spain

8 3. Departamento de Física Aplicada, Universidad de Granada, Granada, Spain

9 4. Andalusian Institute for Earth System Research, Universidad de Granada, Granada, Spain

10 5. Estación de Sondeos Atmosféricos El Arenosillo, INTA, Huelva, Spain

11 6. Évora Geophysics Centre and Dep. Physics, University of Évora, Évora, Portugal

12 7. Universidad Politécnica de Cataluña, Barcelona, Spain

13

14 Corresponding author: D. Mateos, Grupo de Óptica Atmosférica, Universidad de Valladolid, Paseo

15 Belén 7, 47011, Valladolid, Spain. E-mail: mateos@goa.uva.es

16

17

18

19

20   **Abstract**

21   A better understanding of the aerosol radiative properties is a crucial challenge for climate change

22   studies. This study aims to provide a complete characterization of aerosol radiative effects in

23   different spectral ranges within the shortwave (SW) solar spectrum. For this purpose, long-term

24   datasets of aerosol properties from six AERONET stations located in the Iberian Peninsula

25   (Southwestern Europe) are analyzed in term of climatological characterization and trends. Aerosol

26   information is used as input to the libRadtran model in order to determine the aerosol radiative

27   effect at the surface in the ultraviolet (ARE_{UV}), visible (ARE_{VIS}), near-infrared (ARE_{NIR}), and the

28   entire SW range (ARE_{SW}) under cloud-free conditions. Over the whole Iberian Peninsula, yearly

29   aerosol radiative effects in the different spectral ranges are: $-1.1 < ARE_{UV} < -0.7$ W m^{-2}, $-5.7 <$

30    $ARE_{VIS} < -3.5$ W m^{-2}, $-2.6 < ARE_{NIR} < -1.6$ W m^{-2}, and $-8.8 < ARE_{SW} < -5.7$ W m^{-2}. Monthly

31   means of ARE show a seasonal pattern with larger values in spring and summer. The aerosol

32   forcing efficiency (AFE), ARE per unit of aerosol optical depth, is also evaluated in the four

33   spectral ranges. AFE exhibits a dependence on single scattering albedo and a weaker one on

34   Ångström exponent. AFE is larger (in absolute value) for small and absorbing particles. The

35   contributions of the UV, VIS, and NIR ranges to the SW efficiency vary with the aerosol types.

36   Aerosol size determines the fractions of AFE_{VIS}/AFE_{SW} and AFE_{NIR}/AFE_{SW}. VIS range is the

37   dominant region for all types, although non-absorbing large particles cause a more equal

38   contribution of VIS and NIR intervals. The AFE_{UV}/AFE_{SW} ratio shows a higher contribution for

39   absorbing fine particles.

40

41

1. Introduction

Atmospheric aerosol particles can absorb and scatter part of the total amount of solar radiation entering the Earth's atmosphere. In fact, aerosols directly influence the Earth's energy budget and act as cloud condensation nuclei modifying the cloud structure (e.g., Boucher et al., 2013). Aerosols can either be produced by ejection into the atmosphere or by physical and chemical processes within the atmosphere. Aerosol particles affect the radiative field by attenuating the direct component thereby enhancing (or reducing under a highly absorbing aerosol) the diffuse one. They also produce indirect effects by perturbing the Earth's atmospheric radiative balance by modulating cloud albedo and fraction.

The aerosol radiative effect (ARE) is defined as the change in net radiation due to changes in atmospheric aerosol properties and content. This is a key quantity in the determination of climate change (e.g., Hansen et al., 1998). Most studies dealing with ARE have focused on discrete wavelengths, whole shortwave (SW) solar radiation spectrum (e.g., Rajeev and Ramanathan, 2001; García et al., 2008; di Sarra et al., 2008; Foyo-Moreno et al., 2014; Mateos et al., 2013a), longwave (LW) radiation (e.g., Panicker et al., 2008; di Sarra et al., 2011; Antón et al., 2014), ultraviolet (UV) interval (e.g., Hatzianastassiou et al., 2004; Kazadzis et al., 2009; Nikitidou et al., 2013), and visible (VIS) range (e.g., Jayaraman et al., 1998; Horvath et al., 2002; Bush and Valero, 2003; Meloni et al., 2003). With regards to surface SW radiative effect (ARE_{SW}), Di Biagio et al. (2010) obtained the maximum radiative daily effects for different aerosol types in the central Mediterranean in the period 2004-2007: -61 Wm^{-2} (desert dust aerosols), -26 Wm^{-2} (urban/industrial ‑ biomass burning aerosols) and -43 Wm^{-2} (mixed aerosols). All these negative figures point out a cooling of the Earth's surface. Aerosol radiative effects in the LW range (ARE_{LW}) for dust particles are expected to be smaller than in the SW and with positive sign (see, e.g., di Sarra et al., 2011; Antón et al., 2014). Hence, this heating effect at the surface can partly offset the cooling induced in the SW

range. With respect to the ARE for the UV range (ARE_{UV}), Nikitidou et al. (2013) analyzed the ARE in two different spectral regions in the UV range, 300-315 and 315-360 nm. They found a stronger attenuation in the UV-B than in the UV-A.

The main goal of this study is to evaluate the ARE at the surface over the Iberian Peninsula, which is a region of great interest because of its geographical position in Southwestern Europe, near the African continent and the interface between the Atlantic Ocean and the Mediterranean Basin. Thus, it is affected by frequent desert dust intrusions which modulate their aerosol climatology (Toledano et al., 2007a, Bennouna et al., 2011; Pey et al., 2013; Valenzuela et al., 2012). In addition, this area is also affected by a great variety of air masses loaded with different aerosol types: clean continental, polluted plumes of central Europe, and marine aerosols. Hence, aerosol climatology at six stations (Palencia, Barcelona, Cabo da Roca, Évora, Granada, and El Arenosillo) is also carried out for different time periods between 2001 and 2012. Aerosol radiative effects as well as their efficiency are calculated in four regions of the solar spectrum (ultraviolet, visible, near-infrared, and shortwave) and the relative contribution of each range with respect to the whole solar spectrum is analyzed as a function of the aerosol properties. Therefore, this study is intended to contribute to the understanding of the aerosol impact on radiative budget over the Iberian Peninsula.

This article presents the following outline: detailed descriptions of the aerosol stations and the database used are performed in Section 2; Section 3 includes the followed methodology; the results obtained in the different analyses about the climatology of aerosol properties, aerosol radiative effects, and aerosol forcing efficiencies are shown and discussed in Sections 4,5, and 6, respectively. Finally, the main conclusions of this article are summarized in Section 7.

2. Columnar aerosol optical data

The aerosol data are obtained from the Aerosol Robotic Network (AERONET) (Holben et al., 1998). Six AERONET sites operating in the Iberian Peninsula are selected in this study: Palencia, Barcelona, Évora, Cabo da Roca, Granada and El Arenosillo (see Table 1), all of them with a minimum of 8 years of data sets of continuous observations. These sites present the largest records of aerosol properties in the Iberian Peninsula in the AERONET network.

The standard instrument used in AERONET is the Cimel CE-318 radiometer. It performs direct sun measurements at several wavelengths in the spectral range 340-1020 nm. Furthermore, the instrument also measures sky radiance in the solar almucantar and principal plane configurations at 440, 670, 870 and 1020 nm wavelengths. A detailed description of this instrument was provided by Holben et al. (1998). The direct sun observations are used to derive the spectral aerosol optical depth (AOD) and the corresponding Ångström exponent. The sky radiances together with the AOD are employed to retrieve a set of aerosol optical and microphysical properties via inversion methods (Dubovik and King, 2000; Dubovik et al., 2006). These include particle size distribution, complex refractive index, single scattering albedo (SSA), phase function, asymmetry parameter, fraction of non-spherical particles, etc. (see http://aeronet.gsfc.nasa.gov/new_web/Documents/Inversion_products_V2.pdf). Data are provided in three database levels: 1.0 (raw data), 1.5 (cloud-screened) and 2.0 (cloud-screened and quality assured).

The calibration of these instruments is performed following AERONET protocols by AERONET-NASA, PHOTONS and RIMA networks every 12 months of operation approximately. The estimated uncertainty is 0.01-0.02 for AOD (larger at shorter wavelengths) and ~5% for the sky radiances (Holben et al., 1998). The SSA has an absolute uncertainty about 0.03-0.07 depending on the aerosol load and type (Dubovik et al., 2000).

5

113 Level 2.0 aerosol optical depth data have been used in this work. However, it is well-known that

114 when level 2.0 inversion data are used, the number of available observations of single scattering

115 albedo (SSA) and asymmetry factor (g) is quite limited because these variables are only considered

116 reliable when $AOD_{440nm} > 0.4$[1]. Such AOD is mainly reached in the study region during Saharan

117 dust or biomass burning events, therefore we would not have information on SSA and g for other

118 conditions. To solve this issue, we have reduced the threshold of the level 2.0 inversion products.

119 For this, we started with the level 1.5 data (for those quality-assured almucantar data that reached

120 level 2.0) and applied the same criteria used by AERONET to elaborate the level 2.0 regarding the

121 number of symmetrical angles, retrieval error and solar zenith angle (see

122 http://aeronet.gsfc.nasa.gov/new_web/Documents/AERONETcriteria_final1_excerpt.pdf).

123 However, a less restrictive threshold is applied to the AOD, which we restricted to cases with

124 $AOD_{440nm} > 0.15$, instead of 0.4. This choice must be considered a compromise between the amount

125 and the quality of the data. This kind of approach has been adopted by other authors using

126 AERONET absorption data (e.g. Mallet et al., 2013). The threshold of 0.15 seems adequate

127 analyzing the typical values of the AOD in the Iberian Peninsula (e.g., Bennouna et al., 2011;

128 Obregón et al., 2012), because it can be considered a value to separate background aerosol

129 conditions from episodic events with moderate or high aerosol loadings. The level 1.5-filtered data

130 of SSA and g are daily averaged in order to have one value per day. In these conditions, the

131 estimated uncertainty of the single scattering albedo is ±0.05-0.07 (Dubovik et al., 2000).

132 Furthermore, for those days presenting level 2.0 data but also measurements in the 1.5-filtered level,

133 we tested the uncertainty of our approach. We evaluated the difference in the SSA values of the

134 level 1.5-filtered data with respect to the closest level 2.0 data. The mean relative differences in the

---

[1] Other inversion products, like the volume size distributions, are provided for all AOD levels.

135   SSA values between both methodologies are smaller than 1%, being in the same order that the

136   inversion uncertainty.

137   Lastly, when the AOD is low (<0.15 at 440 nm), there is no reliable information on the absorption

138   properties in the almucantar retrievals. Such low AOD is typical in our study region (e.g. almost

139   70% of observations at Palencia, Granada and Évora are below this threshold). If only cases with

140    $AOD_{440nm}>0.15$ are considered in our study, the derived aerosol radiative effect would be

141   unrealistically large. To overcome this problem of representativeness, fixed values of SSA (0.90)

142   and g (0.75) have been used for the cases with AOD < 0.15 at 440 nm, considering typical values

143   for continental, desert, and maritime aerosols (e.g., Hess et al., 1998). In spite of the associated

144   uncertainties, our approximation (daily level 1.5-filtered values of these aerosol properties for AOD

145   > 0.15 together with a typical fixed value for low AOD cases) provides a good characterization of

146   the aerosol absorption of the particles present in the atmosphere. The data products and AERONET

147   database level are summarized in Table 2, where the estimated absolute uncertainties of AOD and

148   SSA are also provided.

149

150   **3. Methodology**

151   The ARE calculations are performed in the ultraviolet (ARE_{UV}, 280-400 nm), visible (ARE_{VIS}, 400-

152   700 nm), near-infrared (ARE_{NIR}, 700-2800 nm), and shortwave (ARE_{SW}, 280-2800 nm) intervals.

153   For this purpose, cloud-free simulations are carried out by means of a radiative transfer code.

154   The libRadtran model (Mayer and Kylling, 2005) has been shown to be a useful tool for obtaining

155   solar radiation data, presenting high accuracy (e.g., Román et al., 2014). Version 1.7 of the

156   libRadtran is used in this study with inputs of aerosol, total ozone column (TOC), precipitable water

157   vapor column (PWC), and surface albedo data. We performed simulations of ultraviolet (280-400

158 nm), visible (400-700 nm), near-infrared (700-2800 nm), and shortwave (280-2800 nm) radiation

159 during the periods indicated in Table 1. Total ozone column is provided by the Ozone Monitoring

160 Instrument (OMI) and Total Ozone Mapping Spectrometer (TOMS). Daily values of these

161 instruments are obtained from the Daily Level 3 Global Gridded products, which are downloaded

162 using the Giovanni application (http://disc.sci.gsfc.nasa.gov/giovanni). Level 2.0 AERONET PWC

163 data are used in the calculations. The uncertainty of this parameter is 10-15% (Holben et al., 1998).

164 In addition, retrievals of surface albedo at 440, 675, 870 and 1020 nm from the AERONET

165 algorithm are also used in this work. For land surface cover, this algorithm relies on the Lie–Ross

166 model (Lucht and Roujean, 2000), but considering the bidirectional reflectance distributions from

167 MODIS (Moody et al., 2005).

168 Aerosol properties obtained from AERONET measurements are also used as input to the libRadtran

169 model. Ångström coefficients, α and β, are utilized to compute a spectral aerosol optical depth in

170 the wavelengths of interest (Schuster et al., 2006). Ångström exponent α is obtained with the

171 measurements between 440 and 870 nm, while the turbidity β is obtained from the α value and

172 aerosol data at 1020 nm. Since the aerosol asymmetry factor, single scattering albedo, and surface

173 albedo are obtained at four wavelengths from AERONET in each measurement, three different

174 spectral regions are simulated with the libRadtran model. For computations in the UV range (280-

175 400 nm), the AERONET retrievals of aerosol asymmetry factor, aerosol single scattering albedo,

176 and surface albedo at 440 nm are used. The AERONET retrievals at 675 nm of the same variables

177 are used in the visible range (400-700 nm), while in the near-infrared region (700-2800 nm) we

178 used the average properties retrieved at 870 and 1020 nm. In each interval, these properties are

179 considered as wavelength independent. This choice to perform the radiative transfer simulations is

180 proven as adequate in the Appendix A. Other options in the model set-up are: extraterrestrial

181 irradiance values are taken from Gueymard (2004); profiles of temperature, air density, ozone and

182 other atmospheric gases are taken from the midlatitude summer/winter standard atmospheres; and

183   the radiative equation solver is the improved version of the discrete ordinate method of Stamnes et

184   al. (2000) (DISORT2) calculated by 16-streams (e.g., de Miguel et al., 2011). After computing the

185   solar irradiance in the different spectral intervals, the SW irradiance is evaluated by adding up the

186   contributions of these three spectral regions.

187   In order to evaluate the aerosol radiative effect, the simulations under aerosol-free conditions are

188   also computed with the same inputs as explained above, but with a fixed β value of 0.001.

189   The use of radiative transfer models fed with reliable experimental aerosol data to determine the

190   ARE has been also employed in other studies (e.g., Barja and Antuña, 2011; Valenzuela et al.,2012;

191   García et al., 2014).

192   Once the simulated radiometric values are obtained, ARE is derived for each interval (X represents

193   UV, VIS, NIR, and SW) at the surface by:

194

195    $$\text{ARE}_X = \left(X_{aer}^{\downarrow} - X_{aer}^{\uparrow} \right) - \left(X_{NOaer}^{\downarrow} - X_{NOaer}^{\uparrow} \right) \qquad (1)$$

196

197   where X_{aer} and X_{NOaer} are the irradiances (W m^{-2}) for the X range under actual and aerosol-free

198   conditions, respectively.

199   Daily values are obtained by the integration of the hourly data during the whole day (24 h)

200   considering ARE = 0 Wm^{-2} for SZA > 90º (e.g., Bush and Valero, 2003; Valenzuela et al., 2012)

201   and assuming cloud-free conditions along the day:

202

$$\text{ARE}_{daily} = \sum \text{ARE}_{hourly} \frac{dt}{24} \qquad (2)$$

203

204   The aerosol forcing efficiency (AFE) is defined as the rate at which the radiative effect varies per

205   unit of AOD (e.g., Di Biagio et al., 2009; and the references therein). The linear relationship

206   between aerosol radiative effect and AOD is well known (see, e.g., Costa et al., 2004, 2006; Di

207   Biagio et al., 2009). Hence, in this study, ARE is obtained as the slope of linear fits in the ARE vs

208   AOD_{500nm} relationships. Therefore, AFE values are expressed in $W\ m^{-2}$ per AOD_{500nm}-unit ($Wm^{-2}\tau^{-1}$

209   ).

210   With respect to the temporal trends calculated in this study, the Sen's method (Sen, 1968) is applied

211   to evaluate the slope of a time series using the Mann-Kendall non parametric test to determine the

212   significance of these rates. The Sen's method is not greatly affected by outliers and can be

213   computed when there are gaps in the database (Collaud Coen et al., 2013). This is a common and

214   adequate method in temporal trend evaluation (e.g., Sánchez-Lorenzo et al., 2013). The trends

215   calculated in this study are obtained in the corresponding physical units per year. However, to unify

216   notation with previous studies dealing with the radiative effect trends of clouds and aerosols (e.g.,

217   Mateos et al., 2013b), the results are multiplied by 10 and expressed in physical units per decade. In

218   this way, the trends are also easier to read.

219

220   **4. Analysis of aerosol properties over the Iberian Peninsula**

221   A direct CIMEL retrieval (AOD at 440 nm) is selected to perform the climatological analysis

222   because the estimations of AOD_{500nm} (used in the ARE calculations) are obtained using α values.

223   Hence, we minimized the impact of other uncertainty sources in the AOD analysis. Besides, the

224   results for AOD_{440nm} and AOD_{500nm} do not differ excessively. In order to identify the differences in

225   the aerosol climatology over the six sites analyzed in this study, the monthly distribution of the

226   daily values of the AOD_{440nm} and α are evaluated using the database mentioned in Table 1. All the

227   available level 2.0 AERONET measurements are used in this section.

228   Figure 1 shows the climatology of the aerosol load by box whisker plots. Several conclusions can

229   be drawn from this figure. The highest values of the AOD occur in Barcelona, as can be expected

230   because it is a large city. With respect to the monthly average values (triangles in the figure), the

231   central stations in the Iberian Peninsula (Palencia and Évora) exhibit AOD_{440nm} below 0.2, while the

232   southern sites (Cabo da Roca, Granada, and El Arenosillo) show aerosol load over 0.2 during

233   summer months. The AOD_{440nm} seasonal distribution is seen, with maximum values in summer and

234   minimum ones in winter. However, the seasonality becomes more evident in the stations outside the

235   central area of the Iberian Peninsula. The large differences between median and average values for

236   some months evidence a large impact of high aerosol optical depth events on the monthly

237   climatology. In this line, the bimodality of the monthly AOD climatology (with two maximum

238   monthly means occurring in March and summer months) observed for the El Arenosillo site has

239   been already reported by previous studies (e.g., Bennouna et al., 2011), and directly attributed to

240   desert dust intrusions from the African continent.

241   To go further in the characterization, α allows for a better understanding of the particle size over

242   each site. Figure 2 shows the climatology of this variable over the six stations using also box

243   whisker plots. Analyzing the monthly average means, α values larger than one, indicative of the

244   predominance of fine particles, are dominant over Barcelona, Palencia, and Évora. The other three

245   stations (Cabo da Roca, Granada, and El Arenosillo) present monthly α averages over and below 1,

246   which means a larger variety of aerosol sizes over these stations. A seasonal dependence over

247   Granada site is seen, with winter months dominated by fine particles and summer months by larger

248   ones (see also Navas-Guzman et al., 2013). Values of α present a large variability during summer

249   which is indicative of the influence of different aerosol types including biomass burning events and

11

250   Saharan dust transport (e.g., Pérez-Ramírez, 2008). The monthly distribution of α is symmetric with

251   similar average and median values through the year for the six sites.

252   With the daily AOD and α values, it is possible to classify the origin of the aerosol particles.

253   Previous studies suggest different thresholds of AOD and α (e.g., Hess et al., 1998; Pace et al.,

254   2006; Toledano et al., 2007b). A simple classification, which can be used for the whole Iberian

255   Peninsula, of aerosol type is carried out in this study. The threshold between fine and large particles

256   is placed at $\alpha = 1$, while the situations with a high aerosol load are those with $AOD_{440nm} > 0.2$.

257   Therefore, aerosol particles can be classified in four types: maritime ($AOD_{440nm} < 0.2$ and $\alpha < 1$),

258   desert dust ($AOD_{440nm} > 0.2$ and $\alpha < 1$), continental clean ($AOD_{440nm} < 0.2$ and $\alpha > 1$), and

259   continental polluted ($AOD_{440nm} > 0.2$ and $\alpha > 1$). Note that the limit of $AOD_{440nm} < 0.2$ is arbitrary

260   and this value could be adjusted according to the sites, which likely produce a different distribution

261   in the pie diagrams. Actually, even close stations can present slight differences in the α-AOD

262   classification (see, e.g., Obregón et al. 2012). However it is not the aim of this work to provide an

263   extensive aerosol climatology, but rather to demonstrate the great variety of air masses over Iberia

264   which transport different aerosol types. Although other types, such as biomass burning or mixed

265   aerosols, are placed in the boundaries of these types, this simple classification can provide

266   information about the aerosol sources for the six sites. The classification used here is in line with

267   the previous studies. For instance, Toledano et al., (2007b) proposed for El Arenosillo site similar

268   thresholds (see their Table V), although they identified continental polluted aerosols with an

269   AOD_{440nm} larger than 0.35 and $\alpha > 1.4$. Pace et al., (2006) proposed at Lampedusa island (Central

270   Mediterranean) a desert dust identification when $AOD_{440nm} \geq 0.15$ and $\alpha \leq 0.5$.

271   Figure 3 shows pie diagrams with the frequency of occurrence of the four aerosol types. The six

272   diagrams agree pointing at continental clean as the main type of aerosols over the Iberian Peninsula.

273   In Barcelona, there is also an important contribution of continental polluted, since Barcelona is a

274   large coastal city with relevant pollution levels from vehicular and ship traffic (e.g., Reche et al.,

275   2011). The influence of maritime aerosols is notable at El Arenosillo, Cabo da Roca, and Évora

276   sites (see also e.g., Bennouna et al., 2011; Obregón et al., 2012). Furthermore, desert dust events are

277   shown to be common in the Iberian Peninsula with a higher occurrence at Granada and El

278   Arenosillo sites (the two closest points to the African continent and hence to the Saharan desert)

279   (see also Toledano et al., 2007b; Guerrero-Rascado et al., 2009; Antón et al., 2012). For instance,

280   the minimum values of α obtained for Granada station during summer months are linked to the

281   higher likelihood of desert dust events (Valenzuela et al., 2012), being sometimes associated with

282   high aerosol loads (Córdoba-Jabonero et al., 2011). These results corroborate the findings obtained

283   by previous studies about desert dust events over the Iberian Peninsula (see, e.g., Lyamani et al.,

284   2005; Toledano et al., 2007b; Cachorro et al., 2008).

285   The inter-annual change of aerosol load can be established over the last decade in the Iberian

286   Peninsula. The yearly values of AOD_{440nm} at the six sites are shown in Figure 4. The geographical

287   distribution of AOD through the Spanish geography is observed in the figure. Barcelona site

288   presents yearly values over ~0.2. Granada, El Arenosillo, and Cabo da Roca exhibit yearly means in

289   the interval between 0.15 and 0.22, while the means for Palencia and Évora sites are slightly lower

290   in the range 0.12-0.18. Analyzing the six sites together, the year of 2010 presents one of the

291   minimum values of AOD_{440nm}, while the maximum averages seem to appear at the early 2000s. The

292   different sampling of AOD measurements in the six sites can produce discrepancies because

293   different events are or are not captured in each database. In addition, possible technical problems

294   and meteorological conditions (CIMEL aerosol data are recorded under cloud-free skies) cause a

295   non-equally distribution through the year. Overall, summer is the season with the largest

296   contribution of data, followed by spring, autumn, and winter. Looking at the years with a large

297   sampling (>200 days in, at least, four stations), 2005, 2007, and 2011, all the features mentioned

298   above are corroborated for these particular years. The minimum of 2010 occurs when two Southern

sites (El Arenosillo and Cabo da Roca) have not enough data to evaluate the yearly mean. Hence, we cannot ensure that the apparent minimum of AOD recorded that year is linked to global-scale phenomena or to more local conditions at the other sites. During 2010 a persistent negative phases of North Atlantic Oscillation (NAO) and Quasi Biennal Oscillation (QBO) indexes was observed (e.g., Steinbrecht et al., 2011), and the connection between air mass transport at global scale and particulate matter (at the surface) is proved by Pey et al., (2013) in the Eastern Iberian Peninsula.

With respect to the temporal change, the evolution of these yearly values seems to be weak, which can be attributed to the large variability observed in the mean values, affected by different conditions and phenomena. In spite of this, the evaluation of the trend rates (see Section 3 for details) produces the more statistically significant trend for the Barcelona site, where a decrease of the aerosol load of 0.09 AOD_{440nm}-unit per decade is observed with a *p value* of 0.02. The *p values* for the other sites point out non-statistically significant trends (*p value* > 0.05). However, the sign of the temporal trends is negative for all of them. Hence, a slight reduction of the aerosol load over the Iberian Peninsula can be deduced since 2000 from the annual values. This result obtained in the Southeastern Europe is in line with the long-term analysis of AOD series performed in Northern Germany and Switzerland by Ruckstuhl et al. (2008). These authors highlight a strong decrease of aerosol load starting in 1985, while the values are stabilized since about 2000.

The reasons behind the decrease in the aerosol load since the early 2000s are a mixed of anthropogenic and natural sources. As was reported by Aas et al. (2013), the particulate matter (PM) emissions in the Iberian Peninsula have decreased around 25% between 2000 and 2011. Furthermore, observational PM data in different Spanish sites have also shown a decrease trend in the 2000s (e.g., Barmpadimos et al., 2012; Cusack et al., 2012; Pey et al., 2013; Bennouna et al., 2014; Mateos et al., 2014). This fact can be understood by the effect of the current economic crisis and the implementation of new environmental laws to control the pollution (e.g., Querol et al.,

323   2014). In addition, recent studies have shown that natural aerosols have also decreased in the last

324   decade. For instance, Gkikas et al. (2013) reported, using satellite AOD estimations, that strong and

325   extreme desert dust episodes in the Mediterranean decreased in the period 2000-2007 over land

326   surfaces. This trend is understood due to the low spring and summer frequencies in 2005 and 2007

327   and the high frequencies in 2000 and 2003. As it was shown by Pey et al. (2013), one possible

328   reason behind this trend is the atypical trajectories followed by the air masses emerging from North

329   Africa in summer since 2006. Hence, both columnar and surface aerosols have pointed out a

330   decrease in the aerosol load over the Iberian Peninsula, which has increased solar radiation levels

331   reaching the surface in the 2000s (Mateos et al., 2014).

332

333   **5. Inter-annual and intra-annual evolution of ARE**

334   From the daily data, the yearly ARE for each station and spectral range is evaluated to analyze the

335   inter-annual changes (see Figure 5). In spite of the high variability of the yearly values with large

336   standard deviations (see the vertical bars for Palencia station in the figure), the radiative effects of

337   atmospheric aerosols have slightly declined over the last years. The patterns of ARE in the UV,

338   VIS, NIR, and SW ranges are similar, since the inter-annual changes are simultaneously observed in

339   the four spectral intervals. With respect to the geographical distribution, Barcelona and Granada

340   sites exhibit the largest effects (more negative ARE), which is in line with the large values of

341   AOD_{440nm} shown in Figure 4. The weakest aerosol effect (less negative ARE) is observed in

342   Palencia and Évora sites, which is again linked to the lower yearly AOD_{440nm}.

343   To establish the general behavior of the ARE over the whole Iberian Peninsula, the yearly values

344   using the six ground-based stations are evaluated. Only those years with, at least, simultaneous

345   measurements at three sites are considered in these averages, and consequently, the time period is

346   limited to 2004-2012. Figure 6 shows the evolution of the ARE and AOD at 500 nm for the entire

15

347   peninsula. The decline of the AOD for this mean series produces a consequent decrease in the

348   aerosol radiative effect at the four spectral ranges. The temporal trends of these yearly values are

349   evaluated, and all the trends shown in Figure 6 resulted with *p values* between 0.004 and 0.03.

350   Overall, ARE_{SW} over the Iberian Peninsula increased 3.6 W m^{-2} per decade (*p value* = 0.028) while

351   the aerosol reduced 0.04 AOD_{500nm}-unit per decade (*p value* = 0.006). Furthermore, this reduction in

352   the radiative effects of the atmospheric aerosol over the Iberian Peninsula could partially contribute

353   to the increase in the levels of SW radiation at the surface (the brightening phenomenon) in this

354   region reported by, e.g., Sanchez-Lorenzo et al. (2013) and Mateos et al. (2013b).

355   The yearly aerosol radiative effects over the entire peninsula are in the ranges: $-1.1 < ARE_{UV} < -0.7$

356   W m^{-2}, $-5.7 < ARE_{VIS} < -3.5$ W m^{-2}, $-2.6 < ARE_{NIR} < -1.6$ W m^{-2}, and $-8.8 < ARE_{SW} < -5.7$ W m^{-2}.

357   The larger contribution of the visible spectral region with respect to the whole solar spectrum was

358   also noticed by Bush and Valero (2003), and this is expected since the maximum of shortwave

359   radiation is found in this interval. The relationship between ARE and AOD_{500nm} is analyzed more in

360   detail in Section 6, when the aerosol forcing efficiency is evaluated for each ground-based station.

361   In addition to the inter-annual changes, the intra-annual behavior is also analyzed. For this purpose,

362   the annual cycle (12 monthly means) is evaluated for the six stations (see Figure 7). A seasonal

363   pattern is seen in ARE_{UV} and ARE_{VIS}, and therefore, ARE_{SW}. However, ARE_{NIR} does not follow a

364   seasonal pattern, particularly at the Évora and Palencia stations given that ARE_{NIR} remains nearly

365   constant. Small differences among the six stations are observed in the annual cycle during the cold

366   seasons. The aerosol radiative effects are stronger during summer months. This can be related to the

367   higher likelihood of desert dust or biomass burning events over the Iberian Peninsula in these

368   months (e.g., Cachorro et al., 2008; Valenzuela et al., 2012), as was mentioned above. This is

369   corroborated by the increase of the differences among the stations during the warm season, likely

370   due to the variability in the impact of the desert dust episodes which strongly depend on the

16

geographical location of each site. The higher occurrence of large aerosol loads during the warm

seasons (see Figure 1), can explain the more negative ARE during summer and spring in Figure 7.

For instance, the Barcelona station, with the largest values of AOD_{440nm}, is the bottom curve of each

panel in Figure 7. Furthermore, the influence of mineral dust aerosol (with high aerosol optical

depth) during these months also causes strong radiative effects, as was also reported by previous

studies (e.g., Cachorro et al., 2008; Guerrero-Rascado et al., 2009; Antón et al., 2011; Román et al.,

2013; García et al., 2014). In addition, the bimodality of the monthly AOD climatology mentioned

in Section 4 has its impact on the radiative effects. The annual AOD cycle (see Figure 1, El

Arenosillo site) causes the inverse monthly distribution of ARE with a first minimum in March.

This effect is more clearly seen in ARE_{NIR} and ARE_{SW}.

6. Aerosol radiative forcing efficiency in different spectral ranges

The daily AFE values are calculated (following the methodology described in Section 3) in all the

spectral ranges. AFE is a function of the aerosol optical properties, where both the aerosol particle

size distribution and absorptive properties play a key role (e.g., Antón et al., 2011). As we assumed

a fixed value of SSA = 0.90 in the simulations with $AOD_{440nm} < 0.15$ (see Table 2), the AFE is

calculated only for those cases showing AOD_{440nm} larger than 0.15.

To identify the influence of SSA and α on AFE, this variable is calculated for several intervals of

each aerosol property. Four categories of single scattering albedo at 675 nm are established in the

calculation of the AFE: $1.0 \geq SSA_1 > 0.95$, $0.95 \geq SSA_2 > 0.90$, $0.90 \geq SSA_3 > 0.85$, and $0.85 \geq$

$SSA_4 > 0.80$. Furthermore, aerosol size is classified in three intervals: $0 \leq \alpha_1 \leq 1$, $1 < \alpha_2 \leq 1.5$, and

$1.5 < \alpha_3 \leq 2$. Note that two intervals in the range of α larger than 1 have been considered. One for

median particles and another one for fine particles, because of the relevant importance of median

size particle (continental or mixed aerosol aerosols types) over the Iberian Peninsula (see Figure 3).

17

395 Although the general classification between fine and coarse particles requires a more refined

396 classification (Schuster et al.,2006; Prats et al., 2011), the more general intervals selected in this

397 study are adequate to perform a study of the aerosol sizes at the six stations together.

398 Figure 8 shows the AFE obtained for the UV (AFE$_{UV}$), VIS (AFE$_{VIS}$), NIR (AFE$_{NIR}$), and SW

399 (AFE$_{SW}$) ranges for all these intervals. The threshold to evaluate the average in each sub-interval is

400 fixed at 10 data points. From these figures it is seen that, the stronger the absorption by aerosols, the

401 stronger their forcing efficiency. That is a decrease in the absolute values of the AFE for increasing

402 SSA and for all particle size. In general, the groups of non-absorbing particles exhibit a good

403 agreement among the six stations (see, for instance, AFE values in all the spectral ranges in the

404 interval $1 < \alpha \le 1.5$). Larger differences are obtained in the case of more absorbing aerosol particles.

405 These can be understood because of the different types of aerosols presented over each site (see

406 Section 4) and the different data numbers. The average AFE values over the whole Iberian

407 Peninsula (considering the six stations together) are presented in Table 3 as a function of α and

408 SSA, separately. The role played by the aerosol size on AFE values is different in the three sub-

409 intervals of the shortwave radiation. AFE$_{UV}$ and AFE$_{VIS}$ are larger (in absolute value) for fine

410 particles, while the opposite occurs in the case of AFE$_{NIR}$. As a result of these mixed effects, AFE$_{SW}$

411 shows also a decrease in its values with increasing α, but this effect is weaker than for the visible

412 and ultraviolet parts. SSA exhibits a more dominant role. As was observed before, the most

413 negative values are achieved for the most absorbing aerosols considered in this study (group 1 of

414 SSA, see Table 3).

415 The average values of forcing efficiency obtained in this study (see Table 3) are in line with those

416 found by other authors. Table 4 summarizes the results obtained by previous studies. It is difficult to

417 assess some features in the comparison with previous reported AFE values, because of the different

418 aerosol types, time periods and methods that are analyzed. Our study presents the evaluation of

419   ARE with six long-term databases of aerosol properties. In spite of that, the values shown in Table

420   3 agree with those of Table 4, but the larger discrepancies are observed with the studies focusing on

421   specific events. Our results match better with the results reported by, e.g., Zhou et al. (2005),

422   Meloni et al. (2005), and Di Biagio et al. (2010). As was noticed by, e.g., Costa et al. (2004, 2006)

423   and Di Biagio et al. (2010), AFE at the surface is larger (in absolute term) for aerosols characterized

424   by smaller and absorbing particles. This result is corroborated by the findings shown in this study.

425   Furthermore, as was pointed out by Di Biagio et al. (2010), the aerosol absorption is the dominant

426   factor on AFE evaluated at the surface.

427   To evaluate the contribution of each spectral range with respect to the shortwave, the dependence of

428   each AFE ratio (VIS to SW and NIR to SW) on SSA and α is shown in Figure 9. AFE_{VIS}/AFE_{SW}

429   and AFE_{NIR}/AFE_{SW} ratios are shown in the figure since their contributions are the dominant.

430   AFE_{UV}/AFE_{SW} ratio can be obtained as 100% minus the sum of the percentage of the two other

431   ranges. As expected, non substantial differences are observed in the behavior of the six stations

432   considered in this study. The NIR contribution becomes more decisive for large particles ($\alpha < 1$). It

433   is expected that larger particles interact more with the longer wavelengths, while the smaller

434   particles present more interaction with the shorter wavelengths. The presence of large particles with

435   low SSA (high absorption) leads to a reduction of the AFE_{NIR}/AFE_{SW} ratio as well as an increase of

436   the AFE_{VIS}/AFE_{SW} ratio. However, for non-absorbing (high SSA) large particles, the

437   AFE_{NIR}/AFE_{SW} ratio increases, and the contributions of the visible and infrared parts become more

438   similar (both around ~40-50%). The difference between AFE_{VIS}/AFE_{SW} and AFE_{NIR}/AFE_{SW}

439   increases for intermediate - fine particles. For these particles, the AFE_{VIS}/AFE_{SW} ratio does not

440   show a dependence on SSA. The smallest contribution of the NIR interval is around ~25% under

441   strong absorbing aerosols and fine particles, while AFE_{VIS}/AFE_{SW} is still over 60%. For this case,

442   the contribution of the ultraviolet range achieves a maximum of ~15%, being almost comparable

19

443 with the near infrared contribution. In summary, aerosol size determines the relevance of VIS-NIR

444 ranges, while SSA plays a key role, particularly, for large particles.

445

446 **7. Conclusions**

447 Six long-term datasets of aerosol properties over the Iberian Peninsula were analyzed and used as

448 input in a radiative transfer model to simulate ultraviolet, visible, near-infrared, and shortwave

449 radiation. The aerosol radiative effect (ARE) and aerosol forcing efficiency (AFE) were calculated.

450 The main conclusions are as follows:

451 1) The annual cycles of AOD and α values of atmospheric aerosols over the six analyzed stations

452 present high variability among them, emphasizing the inhomogeneity of the Iberian Peninsula,

453 mainly due to the different aerosol types over each station. The Barcelona site presents the largest

454 values of AOD, although Southern stations (Granada and El Arenosillo sites) frequently exhibit

455 daily values over 0.2 during summer months. The classification α-AOD has shown that continental

456 (mainly, clean) is the principal type of aerosol over the Iberian Peninsula. However, maritime

457 aerosols are also common in the Cabo da Roca, El Arenosillo and Évora sites. Desert dust events

458 are registered at the six sites, with the highest frequency at Granada and El Arenosillo, but the most

459 relevant feature is the South-North gradient of desert dust load which modulates the aerosol

460 climatology over the Iberian Peninsula.

461 2) In the whole Iberian Peninsula, yearly ARE_{UV} ranges between -1.1 and -0.7 Wm^{-2}, ARE_{VIS}

462 ranges between -5.7 and -3.6 Wm^{-2}, and ARE_{NIR} has values between -2.6 and -1.6 Wm^{-2}. As a

463 result, ARE_{SW} is in the range between -8.8 and -5.7 Wm^{-2}. The temporal trends of ARE_{UV}, ARE_{VIS},

464 ARE_{NIR}, and ARE_{SW} exhibit positive statistically significant trends between 2004 and 2012. For

465 instance, the trend rate for the ARE_{SW} is +3.6 Wm^{-2} per decade (statistically significant at the 95%

466   of significance level). This decrease in the aerosol radiative effects is in line with a slight decrease

467   in the AOD levels in the Iberian Peninsula in the last decade.

468   3) The intra-annual ARE cycle exhibits larger values during the spring and summer months when

469   the likelihood of high aerosol loading over the Iberian Peninsula increases. In general, the annual

470   AOD cycle is driven by the occurrence of Saharan dust events.

471   4) The AFE values at the six stations used in this study are in good agreement. Conditions of high α

472   (small particles predominate) and low SSA (high absorption) lead to the largest negative AFE

473   values. Overall, as an average for the Iberian Peninsula: $AFE_{UV} = -6\ Wm^{-2}\tau^{-1}$, $AFE_{VIS} = -34\ Wm^{-2}\tau^{-1}$,

474     $AFE_{NIR} = -19\ Wm^{-2}\tau^{-1}$, and $AFE_{SW} = -59\ Wm^{-2}\tau^{-1}$.

475   5) The contribution of the ultraviolet, visible, and infrared to total shortwave aerosol forcing

476   efficiency is governed by the aerosol type. In general, the visible part of the spectrum is the most

477   dominant part. Non-absorbing large particles cause a more equal contribution of VIS and NIR

478   intervals, while the UV range shows a higher contribution for absorbing fine particles.

479

480

481   **Appendix A**

482   The two choices in the performance of radiative transfer simulations from the libRadtran code

483   concerning aerosol properties are justified in this section.

484   First at all, as it is mentioned in the text, most of the data present $AOD_{440nm} < 0.15$ (~70% for

485   Palencia, Granada, and Évora sites). For these low values, SSA = 0.9 and g = 0.75 are selected by

486   the representativeness of the local aerosols in the six sites of study (e.g., Cachorro et al., 2010). To

487   analyze possible uncertainties emerging from this choice, the radiative net fluxes are also evaluated

488 for SSA and g values covering the most variety of aerosols observed in the Iberian Peninsula.

489 Hence, $SSA_1 = 0.8$, $SSA_2 = 1.0$, $g_1 = 0.65$, and $g_2 = 0.80$ are selected in this analysis. Four

490 possibilities or scenarios are simulated mixing the two values of the aerosol properties. The

491 radiation obtained in each scenario is compared with the assumed case of SSA = 0.9 and g = 0.75.

492 The two optical properties are also fixed as non-wavelength-dependent in this analysis. The

493 AOD_{440nm} used is 0.15, the worst scenario possible for these cases because the higher the AOD the

494 stronger the impact of aerosol properties. The simulations are performed for the four spectral

495 ranges. Table A1 shows the mean relative difference observed for the four scenarios and two

496 different SZAs (30° and 60°). The assumption considered in this study causes, in the worst possible

497 scenarios, errors in the ARE retrievals (obtained as the expanded errors from the radiative

498 uncertainty) $< 10\%$, $< 6\%$, $< 3\%$, and $< 5\%$ for the UV, VIS, NIR, and SW ranges, respectively. As

499 the cases with $AOD_{440nm} < 0.15$ are the large majority of the Iberian Peninsula, they should be

500 included in the study. The experimental retrievals of SSA and g for these cases with low AOD

501 present large uncertainties, and no reliable information can be used to verify our assumption.

502 Hence, the results of this sensitivity study are adequate. As the SSA influences the diffuse radiation,

503 the worst results are obtained at large SZAs. The impact of g on the net fluxes is very weak. In

504 conclusion, the choice of SSA = 0.9 and g = 0.75 in a clean scenario ($AOD_{440nm} < 0.15$) is proven as

505 adequate because of two reasons: a) representativeness of the local aerosols which can be mixture

506 of different types, and b) the low uncertainty produced in the simulations by SSA and g under these

507 conditions.

508 The choice of fixed SSA and g values within each of the spectral ranges (UV, VIS, and NIR)

509 represented by the CIMEL spectral measurements is also justified here. The aerosol models by

510 Shettle (1989) included in the libRadtran code (see Mayer and Kylling, 2005) are used to evaluate

511 the uncertainty of using this approximation. The continental clean aerosols (most common type in

512 the Iberian Peninsula, see Figure 3), and continental polluted aerosols (also very common, which

513 present an extreme case of absorption) are tested in this analysis. The simulations are performed for

514 the expected spectral behavior of SSA and g following Shettle (1989) and the case of fixed

515 properties in the UV (SSA and g values at 440 nm), VIS (SSA and g values at 675 nm), and NIR

516 intervals (SSA and g average of values at 870 and 1020 nm). Figure A1 presents the evolution of

517 the relative error (considering as reference the net flux with the expected spectral dependence of

518 aerosol properties) for several AOD values between aerosol-free and $AOD_{550nm} = 0.6$. In the case of

519 continental clean aerosols (Figure A1.a), the error of using our assumption is lower than 5% for all

520 SZAs and spectral ranges. Therefore, as the large majority of aerosol particles are of this type, the

521 methodology used and proposed in this study only introduces a relative error below 5% in the

522 majority of the simulations. With respect to the continental polluted aerosols (Figure A1.b), the

523 error increases achieving a maximum around 20% for the UV range and very turbid conditions. For

524 large AOD conditions in the Iberian Peninsula (e.g., $AOD_{550nm} = 0.4$) but with low frequency of

525 occurrence in contrast to $AOD_{440nm} < 0.15$, the error of the SW range is below 5%. However, the

526 UV range is more sensitive to our method and the error is around 15% at SZA = 60º. As it was

527 mentioned above, the errors are larger for large SZAs because of the possible interaction between

528 absorption and scattering processes resulting the diffuse radiation. The visible range is more

529 sensitive to the spectral variations than the NIR interval, which exhibits a maximum error around

530 11% at SZA = 60º and $AOD_{550nm} = 0.6$. The daily net radiative fluxes are also evaluated for the two

531 aerosol types in order to quantify the uncertainty in the final simulated data used in this study. For

532 Palencia site (and the corresponding SZA evolution), a daily value for the June 20th is simulated

533 assuming TOC = 300 DU and PWC = 1 cm. The results for the continental polluted case with

534 $AOD_{440nm} = 0.4$ exhibit differences between the spectral and fixed-band aerosol properties of: 7.5%,

535 5.3%, 4.0%, and 4.8% for the UV, VIS, NIR, and SW intervals. The relative errors for the same

536 intervals with continental clean (and same AOD value) are: 1.9%, 1.2%, 1.4%, and 1.4%,

537 respectively. Therefore, the uncertainty due to fixed optical properties in each spectral range is

23

538 dependent on the aerosol type but the error caused can be considered as acceptable. Since actual

539 aerosols often present mixtures of different types, the uncertainty of using the theoretical spectral

540 evolution for one type (given by an aerosol model) can also produce uncertainties which should be

541 taken into account. Although other aerosol types are not tested in this analysis, a similar behavior

542 can be expected. For instance, for the case of desert dust aerosols, Román et al. (2013) found a

543 slight influence of spectral aerosol absorption properties on UV irradiance analyzing a strong

544 Saharan intrusion over Granada site.

545 Therefore, the two assumptions performed in this study in the simulations are adequate for the

546 evaluation of net fluxes and aerosol radiative effects. The uncertainties that can be introduced in the

547 daily values are acceptable being around or smaller than 5% for the net SW radiation. This

548 uncertainty is usually achieved in clear-sky modeling (e.g., Mateos et al., 2013a).

549

24

References

Aas, W., Espen Yttri, K., Stohl, A., Lund Myhre, C., Karl, M., Tsyro, S., Marečková, K., Wankmüller, R., Klimont, Z., Heyes, C., Alastuey, A., Querol, X., Pérez, N., Moreno, T., Lucarelli, F., Areskoug, H., Balan, V., Cavalli, F., Putaud, J.P., Cape J.N., Catrambone, M., Ceburnis, D., Conil, S., Gevorgyan, L., Jaffrezo, J.L., Hueglin, C., Mihalopoulos, N., Mitosinkova, M., Riffault, V., Sellegri, K., Spindler, G., Schuck, T., Pfeffer, U., Breuer, L., Adolfs, D., Chuntonova, L., Arabidze, M., and Abdulazizov, E.: Transboundary particulate matter in Europe Status report 2013, EMEP Report, 4/2013 (Ref. O-7726), ISSN: 1504-6109 (print), 1504-6192 (online), 2013.

Antón, M., Gil, J.E., Fernández-Gálvez, J., Lyamani, H., Valenzuela, A., Foyo-Moreno, I., Olmo, F. J., and Alados-Arboledas, L.: Evaluation of the aerosol forcing efficiency in the UV erythemal range at Granada, Spain, J. Geophys. Res., 116, D20214, doi:10.1029/2011JD016112, 2011.

Antón, M., Valenzuela, A., Cazorla, A., Gil, J.E., Fernández-Gálvez, J., Lyamani, H., Foyo-Moreno, I., Olmo, F.J., Alados-Arboledas, L.: Global and diffuse shortwave irradiance during a strong desert dust episode at Granada (Spain), Atmos. Res., 118, 232–239, doi:10.1016/j.atmosres.2012.07.007, 2012.

584 Antón, M., Valenzuela, A., Mateos, D., Alados, I., Foyo-Moreno, I., Olmo, F.J., Alados-Arboledas,

585   L.: Lonwave aerosol radiative effects during an extreme desert dust event in Southeastern

586   Spain, Atmos. Res., doi: 10.1016/j.atmosres.2014.05.022, 2014.

587 Barja, B., and Antuña, J.C.: The effect of optically thin cirrus clouds on solar radiation in

588   Camagüey Cuba. Atmos. Chem. Phys., 11, 8625–8634, doi:10.5194/acp-11-8625-2011, 2011.

589 Barmpadimos, I., Keller, J., Oderbolz, D., Hueglin C., and Prèvôt, A.S.H.: One decade of parallel

590   fine ($PM_{2.5}$) and coarse (PM_{10}- $PM_{2.5}$) particulate matter measurements in Europe: trends and

591   variability, Atmos. Chem. Phys. 12, 3189-3203, doi: 10.5194/acp-12.3189-2012, 2012.

592 Bennouna, Y., Cachorro, V., Toledano, C., Berjón, A., Prats, N., Fuertes, D., Gonzalez, R.,

593   Rodrigo, R., Torres, B., and de Frutos, A.: Comparison of atmospheric aerosol climatologies

594   over southwestern Spain derived from AERONET and MODIS, Rem. Sen. Env. 115, 1272-

595   1284, 2011.

596 Bennouna, Y.S., Cachorro, V., Burgos, M.A., Toledano, C., Torres, B., and de Frutos, A.:

597   Relationships between columnar aerosol optical properties and surface Particulate Matter

598   observations in north-central Spain from long-term records (2003-2011), Atmos. Meas. Tech.

599   Discuss., 7, 5829-5882, doi:10.5194/amtd-7-5829-2014, 2014.

600 Boucher, O., Randall, D., Artaxo, P., Bretherton, C., Feingold, G., Forster, P., Kerminen, V.-M.,

601   Kondo, Y., Liao, H., Lohmann, U., Rasch, P., Satheesh, S.K., Sherwood, S., Stevens, B., and

602   Zhang, X.Y.: Clouds and aerosols. In Climate Change 2013: The Physical Science Basis.

603   Contribution of Working Group I to the Fifth Assessment Report of the Intergovernmental

604   Panel on Climate Change. T.F. Stocker, D. Qin, G.-K. Plattner, M. Tignor, S.K. Allen, J.

605   Doschung, A. Nauels, Y. Xia, V. Bex, and P.M. Midgley, Eds. Cambridge University Press,

606   571-657, 2013.

607   Bush, B. C., and Valero, F. P. J.: Surface aerosol radiative forcing at Gosan during the ACE– Asia

608   campaign, J. Geophys. Res., 108(D23), 8660, doi:10.1029/2002JD003233, 2003.

609   Cachorro, V. E., Toledano, C., Prats, N., Sorribas, M., Mogo, S., Berjón, A., Torres, B., Rodrigo,

610   R., de la Rosa, J., and De Frutos, A. M.: The strongest desert dust intrusion mixed with smoke

611   over the Iberian Peninsula registered with Sun photometry, J. Geophys. Res., 113, D14S04,

612   doi:10.1029/2007JD009582, 2008.

613   Cachorro, V. E., Toledano, C., Antón, M., Berjón, A., de Frutos, A., Vilaplana, J. M., Arola, A., and

614   Krotkov, N. A.: Comparison of UV irradiances from Aura/Ozone Monitoring Instrument

615   (OMI) with Brewer measurements at El Arenosillo (Spain) – Part 2: Analysis of site aerosol

616   influence, Atmos. Chem. Phys., 10, 11867-11880, doi:10.5194/acp-10-11867-2010, 2010.

617   Collaud Coen, M., Andrews, E., Asmi, A., Baltensperger, U., Bukowiecki, N., Day, D., Fiebig, M.,

618   Fjaeraa, A. M., Flentje, H., Hyvärinen, A., Jefferson, A., Jennings, S. G., Kouvarakis, G.,

619   Lihavainen, H., Lund Myhre, C., Malm, W. C., Mihapopoulos, N., Molenar, J. V., O'Dowd, C.,

620   Ogren, J. A., Schichtel, B. A., Sheridan, P., Virkkula, A., Weingartner, E., Weller, R., and

621   Laj, P.: Aerosol decadal trends – Part 1: In-situ optical measurements at GAW and IMPROVE

622   stations, Atmos. Chem. Phys., 13, 869-894, doi:10.5194/acp-13-869-2013, 2013.

623   Córdoba-Jabonero, C., Sorribas, M., Guerrero-Rascado, J.L., Adame, J.A., Hernández, Y.,

624   Lyamani, H., Cachorro, V., Gil, M., Alados-Arboledas, L., Cuevas, E., and de la Morena, B.:

625   Synergetic monitoring of Saharan dust plumes and potential impact on surface: a case study of

626   dust transport from Canary Islands to Iberian Peninsula, Atmos. Chem. Phys., 11, 3067-3091,

627   doi:10.5194/acp-11-3067-2011, 2011.

628 Costa, M. J., Levizzani, V., and Silva, A. M.: Aerosol Characterization and Direct Radiative

629   Forcing Assessment over the Ocean. Part II: Application to Test Cases and Validation. J. Appl.

630   Meteor., 43, 1818–1833, doi: http://dx.doi.org/10.1175/JAM2157.1, 2004.

631 Costa, M.J., Sohn, B.J., Levizzani, V., and Silva, A.M.: Radiative forcing of Asian dust determined

632   from the synergized GOME and GMS satellite data - A case study, J. Meteorol. Soc. Jpn.,

633   84(1), 85-95, doi: 10.2151/jmsj.84.85, 2006.

634 Cusack, M., Alastuey, A., Pérez, N., Pey, J., and Querol, X.: Trends of particulate matter ($PM_{2.5}$)

635   and chemical composition at a regional site in the Western Mediterranean over the last nine

636   years (2002-2010), Atmos. Env. 12, 8341-8357, doi: 10.5194/acp-12-8341-2012, 2012.

637 de Miguel, A., Mateos, D., Bilbao, J., and Román, R.: Sensitivity analysis of ratio between

638   ultraviolet and total shortwave solar radiation to cloudiness, ozone, aerosols and precipitable

639   water, Atmos. Res., 102, 136–144, doi:10.1016/j.atmosres.2011.06.019., 2011.

640 Di Biagio, C., di Sarra, A., Meloni, D., Monteleone, F., Piacentino, S., and Sferlazzo, D.:

641   Measurements of Mediterranean aerosol radiative forcing and influence of the single scattering

642   albedo, J. Geophys. Res., 114, D06211, doi:10.1029/2008JD011037, 2009.

643 Di Biagio, C., di Sarra, A., and Meloni, D.: Large atmospheric shortwave radiative forcing by

644   Mediterranean aerosols derived from simultaneous ground-based and spaceborne observations

645   and dependence on the aerosol type and single scattering albedo, J. Geophys. Res., 115,

646   D10209, doi:10.1029/2009JD012697, 2010.

647 di Sarra, A., Pace, G, Meloni, D., De Silvestri, L., Piacentino, S., and Monteleone, F.: Surface

648   shortwave radiative forcing of different aerosol types in the Mediterranean, Geophys. Res.

649   Lett., 35, L02714, doi:10.1029/2007GL032395, 2008.

650   di Sarra, A., Di Biagio, C., Meloni, D., Monteleone, F., Pace, G., Pugnaghi, S., and Sferlazzo, D.:

651   Shortwave and longwave radiative effects of the intense Saharan dust event of 25–26 March

652   2010 at Lampedusa (Mediterranean Sea), J. Geophys. Res., 116, D23209,

653   doi:10.1029/2011JD016238, 2011.

654   Díaz, A. M., García, O.E., Díaz, J.P., Expósito, F.J., Utrillas, M.P., Martínez-Lozano, J.A., Alados-

655   Arboledas, L., Olmo, F.J., Lorente, J., Cachorro, V., Horvath, H., Labajo, A., Sorribas, M.,

656   Vilaplana, J.M., Silva, A.M., Elias, T., Pujadas, M., Rodrigues, J.A., and González, J.A.:

657   Aerosol radiative forcing efficiency in the UV region over southeastern Mediterranean:

658   VELETA2002 campaign, J. Geophys. Res., 112, D06213, doi:10.1029/2006JD007348, 2007.

659   Dubovik, O., and King, M.D.: A flexible inversion algorithm for retrieval of aerosol optical

660   properties from Sun and sky radiance measurements, J. Geophys. Res., 105, 20673-20696,

661   2000.

662   Dubovik, O., Smirnov, A., Holben, B.N., King, M.D., Kaufman, Y.J., Eck, T.F., and Slutsker, I.:

663   Accuracy assessments of aerosol optical properties retrieved from Aerosol Robotic Network

664   (AERONET) Sun and sky radiance measurements, J. Geophys. Res., 105, 9791-9806, 2000.

665   Dubovik, O., Sinyuk, A., Lapyonok, T., Holben, B.N., Mishchenko, M., Yang, P., Eck, T.F.,

666   Volten, H., Muñoz, O., Veihelmann, B., van der Zande, W.J., Leon, J.F., Sorokin, M., and

667   Slutsker, I.: Application of spheroid models to account for aerosol particle nonsphericity in

668   remote sensing of desert dust, J. Geophys. Res., 111, D11208, 2006.

669   Esteve, A.R., Estellés, V., Utrillas, M.P., and Martínez-Lozano, J.A.: Analysis of the aerosol

670   radiative forcing over a Mediterranean urban coastal site, Atmos. Res., 137, 194-204,

671   http://dx.doi.org/10.1016/j.atmosres.2013.10.009, 2014.

672 Foyo-Moreno, I., Alados, I., Antón, M., Fernández-Gálvez, J., Cazorla, A., and Alados-Arboledas,

673   L.: Estimating aerosol characteristics from solar irradiance measurements at an urban location

674   in Southeastern Spain, J. Geophys. Res. Atmos., 119, 1845–1859, doi:10.1002/2013JD020599,

675   2014.

676 García, O. E., Díaz, A. M., and Expósito, F. J.: Validation of AERONET estimates of atmospheric

677   solar fluxes and aerosol radiative forcing by ground-based broadband measurements, J.

678   Geophys. Res., 113, D21207, doi:10.1029/2008JD010211, 2008.

679 García, R.D., García, O.E., Cuevas, E., Cachorro, V.E., Romero-Campos, P.M., Ramos, R., and de

680   Frutos, A.M.: Solar radiation measurements compared to simulations at the BSRN Izaña

681   station: Mineral dust radiative forcing and efficiency study, J. Geophys. Res. Atmos., 119, 179–

682   194, doi:10.1002/2013JD020301, 2014.

683 Gkikas, A., Hatzianastassiou, N., Mihalopoulos, N., Katsoulis, V., Kazadzis, S., Pey, J., Querol, X.,

684   and Torres, O.: The regime of intense desert dust episodes in the Mediterranean based on

685   contemporary satellite observations and ground measurements, Atmos. Chem. Phys., 13,

686   12135-12154, doi:10.5194/acp-13-12135-2013, 2013.

687 Guerrero-Rascado, J.L., Olmo, F. J., Avilés-Rodríguez, I., Navas-Guzmán, F., Pérez-Ramírez, D.,

688   Lyamani, H., and Alados-Arboledas, L.: Extreme Saharan dust event over the southern Iberian

689   Peninsula in September 2007: active and passive remote sensing from surface and Satellite,

690   Atmos. Chem. Phys., 9, 8453–8469, doi:10.5194/acp-9-8453-2009, 2009.

691 Gueymard, C.: The sun's total and spectral irradiance for solar energy applications and solar

692   radiation models, Sol. Energy, 76, 423-453, 2004.

693   Hansen, J. E., Sato, M., Lacis, A., Ruedy, R., Tegen, I., and Matthews, E.: Climate forcings in the

694   industrial era, Proc. Natl. Acad. Sci. U.S.A., 95, 12753–12758, doi:10.1073/pnas.95.22.12753,

695   1998.

696   Hatzianastassiou, N., Katsoulis, B., and Vardavas, I.: Global distribution of aerosol direct radiative

697   forcing in the ultraviolet and visible arising under clear skies, Tellus B, 56, 51–71,

698   doi:10.1111/j.1600-0889.2004.00085.x, 2004.

699   Hess, M., Koepke, P., and Schult, I.: Optical Properties of Aerosols and Clouds: The Software

700   Package OPAC, Bull. Am. Meteorol. Soc., 79, 831-844, 1998.

701   Holben, B.N., Eck, T.F., Slutsker, I., Tanré, D., Buis, J.P., Setzer, A., Vermote, E., Reagan, J.A.,

702   KAufman, Y.J., Nakajima, T., Lavenu, F., Jankowiak, I., and Smirnov, A.: AERONET – A

703   federated instrument network and data archive for aerosol characterization, Rem. Sen. Environ.,

704   66, 1–16, 1998.

705   Horvath, H., Alados Arboledas, L., Olmo, F. J., Jovanovic, O., Gangl, M., Kaller, W., Sánchez, C.,

706   Sauerzopf, H., and Seidl, S.: Optical characteristics of the aerosol in Spain and Austria and its

707   effect on radiative forcing, J. Geophys. Res., 107(D19), 4386, doi:10.1029/2001JD001472,

708   2002.

709   Jayaraman, A., Lubin, D., Ramachandran, S., Ramanathan, V. , Woodbridge, E., Collins, W. D.,

710   and Zalpuri, K. S.: Direct observations of aerosol radiative forcing over the tropical Indian

711   Ocean during the Janauary–February 1996 pre-INDOEX cruise, J. Geophys. Res., 103, 13,827–

712   13,836, doi:10.1029/98JD00559, 1998.

713   Kazadzis, S., Kouremeti, N., Bais, A., Kazantzidis, A., and Meleti, C.: Aerosol forcing efficiency in

714   the UVA region from spectral solar irradiance measurements at an urban environment, Ann.

715   Geophys., 27, 2515–2522, doi:10.5194/angeo-27-2515-2009, 2009.

716   Lucht, W. and Roujean, J.L.: Consideration in parametric modelling of BRDF and albedo from

717   multi-angular satellite sensors observations, Remote Sens. Rev., 18, 343–379, 2000.

718   Lyamani, H., Olmo, F.J., and Alados-Arboledas, L.: Saharan dust outbreak over southeastern Spain

719   as detected by sun photometer, Atmos. Env., 39, 7276-7284,

720   doi:10.1016/j.atmosenv.2005.09.011, 2005.

721   Lyamani, H., Olmo, F. J., Alcántara, A., and Alados-Arboledas, L.: Atmospheric aerosols during

722   the 2003 heat wave in southeastern Spain II: Microphysical columnar properties and radiative

723   forcing, Atmos. Environ., 40, 6465–6476, doi:10.1016/j.atmosenv.2006.04.047, 2006.

724   Mallet, M., Dubovik, O., Nabat, P., Dulac, F., Kahn, R., Sciare, J., Paronis, D., and Leon, J.F.:

725   Absorption properties of Mediterranean aerosols obtained from multi-year ground-based

726   remote sensing observations, Atmos. Chem. Phys., 13, 9195-9210, doi:10.5194/acp-13-9195-

727   2013, 2013.

728   Mateos, D., Antón, M., Valenzuela, A., Cazorla, A., Olmo, F.J., and Alados-Arboledas, L.: Short-

729   wave radiative forcing at the surface for cloudy systems at a midlatitude site, Tellus B, 65,

730   21069, http://dx.doi.org/10.3402/tellusb.v65i0.21069, 2013a.

731   Mateos, D., Antón, M., Sanchez-Lorenzo, A., Calbó, J., and Wild, M.: Long-term changes in the

732   radiative effects of aerosols and clouds in a mid-latitude region (1985–2010), Global Planet.

733   Change, 111, 288-295, http://dx.doi.org/10.1016/j.gloplacha.2013.10.004, 2013b.

734   Mateos, D., Sanchez-Lorenzo, A., Antón, M., Cachorro, V.E., Calbó, J., Costa, M.J., Torres, B., and

735   Wild, M.: Quantifying the respective roles of aerosols and clouds in the strong brightening

736   since the early 2000s over the Iberian Peninsula, J. Geophys. Res. Atmos., 119, 10382–10393,

737   doi:10.1002/2014JD022076, 2014.

738 Mayer, B., and Kylling, A.: Technical note: The libRadtran software package for radiative transfer

739   calculations – description and examples of use, Atmos. Chem.Phys., 5, 1855–1877, 2005.

740 Meloni, D., di Sarra, A., DeLuisi, J., Di Iorio, T., Fiocco, G., Junkerman, W., and Pace, G.:

741   Tropospheric aerosols in the Mediterranean: 2. Radiative effects through model simulations and

742   measurements, J. Geophys. Res., 108(D10), 4317, doi:10.1029/2002JD002807, 2003.

743 Meloni, D., di Sarra, A., Di Iorio, T., and Fiocco, G.: Influence of the vertical profile of Saharan

744   dust on the visible direct radiative forcing, J. Quant. Spectrosc. Radiat. Transfer, 93, 397–413,

745   2005.

746 Moody, E.G., King, M.D., Platnick, S., Schaaf, C.B., and Gao, F.: Spatially complete global

747   spectral surface albedos: value-added datasets derived from Terra MODIS land products, IEEE

748   T. Geosci. Remote., 43, 144–158, 2005.

749 Navas-Guzmán, F., Bravo-Aranda, J.A., Guerrero-Rascado, J.L., Granados-Muñoz, M.J., and

750   Alados-Arboledas, L.: Statistical analysis of aerosol optical properties retrieved by Raman lidar

751   over Southeastern Spain, Tellus B, 65, 21234, http://dx.doi.org/10.3402/tellusb.v65i0.21234,

752   2013.

753 Nikitidou, E., Kazantzidis, A., De Bock, V., and De Backer, H.: The aerosol forcing efficiency in

754   the UV region and the estimation of single scattering albedo at a typical West European site,

755   Atmos. Env., 69, 313-320, doi:http://dx.doi.org/10.1016/j.atmosenv.2012.12.035, 2013.

756 Obregón M.A., Pereira S, Wagner F, Serrano A, Cancillo ML, Silva AM.: Regional differences of

757   column aerosol parameters in western Iberian Península, Atmos. Environ., 62, 208-219, doi:

758   10.1016/j.atmosenv.2012.08.016, 2012

759   Pace, G., di Sarra, A., Meloni, D., Piacentino, S., and Chamard, P.: Aerosol optical properties at

760   Lampedusa (central Mediterranean): 1. Influence of transport and identification of different

761   aerosol types, Atmos. Chem. Phys., 6, 697‒713, 2006.

762   Panicker, A. S., Pandithurai, G., Safai, P. D., and Kewat, S.: Observations of enhanced aerosol

763   longwave radiative forcing over an urban environment, Geophys. Res. Lett., 35, L04817,

764   doi:10.1029/2007GL032879, 2008.

765   Pérez-Ramírez, D., Aceituno, J., Ruiz, B., Olmo, F.J., and Alados-Arboledas, L.: Development and

766   calibration of a star photometer to measure the aerosol optical depth: Smoke observations at a

767   high mountain site, Atmos. Env. 42(11), 2733–2738, 2008.

768   Pey, J., Querol, X, Alastuey, A., Forastiere, F, and Stafoggia, M. African dust outbreaks over the

769   Mediterranean Basin during 2001–2011: PM_{10} concentrations, phenomenology and trends, and

770   its relation with synoptic and mesoscale meteorology, Atmos. Chem. Phys., 13, 1395-1410,

771   doi:10.5194/acp-13-1395-2013, 2013.

772   Prats, N., Cachorro, V.E., Berjón, A., Toledano, C., and De Frutos, A.M.: Column-integrated

773   aerosol microphysical properties from AERONET Sun photometer over south-western Spain.

774   Atmos. Chem. Phys. 11, 12353-12547, doi:10.5194/acpd-11-12353-2011, 2011.

775   Querol, X., Alastuey, A., Pandolfi, M., Reche, C., Pérez, N., Minguillón, M.C., Moreno, T., Viana,

776   M., Escudero, M., Orio, A., Pallarés, M., and Reina, F.: 2001-2012 trends of air quality in

777   Spain, Sci. Total Environ., 490, 957-969, 2014.

778   Rajeev, K., and Ramanathan, V.: Direct observations of clear-sky aerosol radiative forcing from

779   space during the Indian Ocean Experiment, J. Geophys. Res., 106, 17,221–17,235,

780   doi:10.1029/2000JD900723, 2001.

781   Reche, C., Viana, M., Moreno, T., Querol, X., Alastuey, A., Pey, J., Pandolfi, M., Prèvôt, A., Mohr,

782   C., Richard, A., Artiñano, B., Gomez-Moreno, F.J., and Cots, N.: Peculiarities in atmospheric

783   particle number and size-resolved speciation in an urban area in the western Mediterranean:

784   Results   from   the   DAURE   campaign,   Atmos.   Env.,   45,   5282-5293,

785   doi:10.1016/j.atmosenv.2011.06.059, 2011.

786   Román, R., Antón, M., Valenzuela, A., Gil, J.E., Lyamani, H., de Miguel, A., Olmo, F.J., Bilbao, J.,

787   and Alados-Arboledas, L.: Evaluation of the desert dust effects on global, direct, and diffuse

788   spectral   ultraviolet   irradiance,   Tellus   B,   65,   19578,

789   http://dx.doi.org/10.3402/tellusb.v65i0.19578, 2013.

790   Román, R., Bilbao, J., and de Miguel, A.: Solar radiation simulations in the Iberian Peninsula:

791   Accuracy and sensitivity to uncertainties in inputs of a radiative transfer model, J. Quant.

792   Spectrosc. Ra., 145, 95-109, 2014.

793   Ruckstuhl, C., Philipona, R., Behrens, K., Coen M.C., Dürr, B., Heimo, A., Mätzler, C., Nyeki, S.,

794   Ohmura, A., Vuilleumier, L., Weller, M., Wehrli, C., and Zelenka, A.: Aerosol and cloud

795   effects on solar brightening and the recent rapid warming, Geophys. Res. Lett., 35, L12708,

796   doi:10.1029/2008GL034228, 2008.

797   Saha, A., Mallet, M., Roger, J. C., Dubuisson, P., Piazzola, J., and Despiau, S.: One year

798   measurements of aerosol optical properties over an urban coastal site: Effect on local direct

799   radiative forcing, Atmos. Res., 90, 195–202, doi:10.1016/j.atmosres.2008.02.003, 2008.

800   Sanchez-Lorenzo, A., Calbó, J., and Wild, M.: Global and diffuse solar radiation in Spain: Building

801   a homogeneous dataset and assessing trends, Global Planet. Change, 100, 343-352,

802   http://dx.doi.org/10.1016/j.gloplacha.2012.11.010, 2013.

803 Santos, D., Costa, M. J., and Silva, A. M.: Direct SW aerosol radiative forcing over Portugal,

804   Atmos. Chem. Phys., 8, 5771–5786, doi:10.5194/acp-8-5771-2008, 2008.

805 Schuster, G. L., Dubovik, O., and Holben, B. N.: Angstrom exponent and bimodal aerosol size

806   distributions, J. Geophys. Res., 111, D07207, doi:10.1029/2005JD006328, 2006.

807 Sen, P. K.: Estimates of the regression coefficient based on Kendall's tau, J. Am., Stat. Assoc., 63,

808   1379–1389, 1968.

809 Shettle, E. P.: Models of aerosols, clouds and precipitation for atmospheric propagation studies,

810   paper presented at Conference on Atmospheric Propagation in the UV, Visible, IR and MM-

811   Region and Related System Aspects, NATO Adv. Group for Aerosp. Res. and Dev.,

812   Copenhagen, 1989.

813 Stamnes, K., Tsay, S.C., Wiscombe, W., and Laszlo, I.: DISORT, a General-Purpose Fortran

814   Program for Discrete-Ordinate-Method Radiative Transfer in Scattering and Emitting Layered

815   Media: Documentation of Methodology, Tech. rep. Dept. of Physics and Engineering Physics,

816   Stevens Institute of Technology, Hoboken, NJ 07030, 2000.

817 Steinbrecht, W., Köhler, U., Claude, H., Weber, M., Burrows, J.P., and van der A, R.J.: Very high

818   ozone columns at northern mid-latitudes in 2010, Geophys Res Lett, 38, L06803,

819   doi:10.1029/2010GL046634, 2011.

820 Toledano, C., Cachorro, V.E., Berjon, A., de Frutos, A.M., Sorribas, M., de la Morena, B., and

821   Goloub, P.: Aerosol optical depth and Ångström exponent climatology at El Arenosillo

822   AERONET site (Huelva, Spain), Q. J. R. Meterol. Soc., 133, 795-807, 2007a.

823 Toledano, C., Cachorro, V.E., de Frutos, A.M., Sorribas, M., Prats, N., and de la Morena, B.:

824   Inventory of African desert dust events over the southwestern Iberian Peninsula in 2000-2005

825   with an AERONET Cimel Sun photometer, J. Geophys. Res. 112, doi:10.1029/2006JD008307,

826   2007b.

827 Valenzuela, A., Olmo, F.J., Lyamani, H., Antón, M., Quirantes, A., and Alados-Arboledas, L.:

828   Aerosol radiative forcing during African desert dust events (2005-2010) over Southeastern

829   Spain, Atmos. Chem. Phys. 12, 10331–10351, doi:10.5194/acp-12-10331-2012, 2012.

830 Zhou, M., Yu, H., Dickinson, R. E., Dubovik, O., and Holben, B. N.: A normalized description of

831   the direct effect of key aerosol types on solar radiation as estimated from Aerosol Robotic

832   Network aerosols and Moderate Resolution Imaging Spectroradiometer albedos, J. Geophys.

833   Res., 110, D19202, doi:10.1029/2005JD005909, 2005.

834

835 Tables

836
837 **Table 1.** Coordinates and time interval of the six AERONET sites used in this study.

Station	Latitude (ºN)	Longitude (ºE)	Altitude a.s.l. (m)	Time interval
Palencia	41.99	-4.52	750	2003-2012
Barcelona	41.39	2.12	125	2004-2012
Cabo da Roca	38.78	-9.50	140	2003-2011
Évora	38.57	-7.91	293	2005-2012
Granada	37.16	-3.61	680	2004-2012
El Arenosillo	37.11	-6.73	0	2000-2009

838
839
840
841
842 **Table 2.** Summary of AERONET data used for ARE calculations: aerosol optical depth (AOD),
843 single scattering albedo (SSA), asymmetry factor (g), precipitable water vapor column (PWC).
844 Estimated absolute uncertainty of AOD and SSA is given according to Dubovik et al. (2002), and
845 PWC error from Holben et al. (1998).

	AERONET database	Estimated uncertainty
AOD	Level 2.0	±0.01-0.02
SSA, g ($AOD_{440} > 0.4$)	Level 2.0	±0.03 (in SSA)
SSA, g ($0.15 < AOD_{440} < 0.4$)	Level 1.5-filtered*	±0.05-0.07 (in SSA)
SSA, g ($AOD_{440} < 0.15$)	Fixed value	
PWC	Level 2.0	10-15%

846 *Filters applied are the same as in level 2.0 except for AOD_{440} (see text).

847
848
849
850
851 **Table 3.** AFE values and their standard error for the UV, VIS, NIR, and SW ranges for, separately,
852 four SSA and three α intervals over the Iberian Peninsula. Units are $Wm^{-2}\tau^{-1}$. SSA groups: $0.85 \geq$
853 $SSA_1 > 0.80$ (group 1), $0.90 \geq SSA_2 > 0.85$ (group 2), $0.95 \geq SSA_3 > 0.90$ (group 3), and $1.0 \geq$
854 $SSA_4 > 0.95$ (group 4); and α groups: $0 \leq \alpha_1 \leq 1$ (group 1), $1.0 \leq \alpha_2 \leq 1.5$ (group 2), and $1.5 < \alpha_3 \leq 2$
855 (group 3). The average values without any classification are also presented.

856

Variable	Group	AFE_{UV}	AFE_{VIS}	AFE_{NIR}	AFE_{SW}
	1	-5.41 ± 0.06	-30.1 ± 0.3	-20.9 ± 0.2	-56.5 ± 0.5
α	2	-6.60 ± 0.09	-38.3 ± 0.4	-19.1 ± 0.2	-64.0 ± 0.6
	3	-7.06 ± 0.10	-39.4 ± 0.4	-16.9 ± 0.2	-63.3 ± 0.7
	1	-9.7 ± 0.2	-52.8 ± 0.8	-24.9 ± 0.5	-87.4 ± 1.4
SSA	2	-8.19 ± 0.10	-44.6 ± 0.4	-21.2 ± 0.2	-74.0 ± 0.6
	3	-6.37 ± 0.05	-35.9 ± 0.2	-19.5 ± 0.2	-61.8 ± 0.3
	4	-4.59 ± 0.05	-26.6 ± 0.2	-18.1 ± 0.2	-49.3 ± 0.3
Average		-5.98 ± 0.05	-33.7 ± 0.2	-19.34 ± 0.11	-59.1 ± 0.3

857
858

Table 4. Daily Forcing Efficiencies at the surface by previous studies. Legend: desert dust (DD), continental-biomass burning (C-BB), and forest fires (FF).

Reference	Aerosol Type	AFE_X	Value $(Wm^{-2}\tau^{-1})$	Time period	Region	More info.
Díaz et al. (2007)	Mixed	AFE_{UV}	-3	July 2002	Spain	290-363 nm
Meloni et al. (2005)	DD Mixed	AFE_{VIS}	-28.4 -45.6	July 2002	Central Mediterranean	
Lyamani et al. (2006)	Mixed	AFE_{VIS}	-75.8	August 2003	Spain	2003 heat wave
Di Biagio et al. (2010)	DD C-BB Mixed	AFE_{SW}	-68.9 -59.0 -94.9	2004-2007	Central Mediterranean	At the equinox
Esteve et al. (2014)	Mixed	AFE_{SW}	-139.0	2003-2011	Spain	200 cloud-free days
Santos et al. (2008)	FF	AFE_{SW}	-113.0	2004-2005	Portugal	Absorbing aerosols
di Sarra et al. (2011)	DD	AFE_{SW}	-55	25-26/03/2010	Central Mediterranean	Strong event
García et al. (2014)	DD	AFE_{SW}	-59	2009-2012	Canary Islands	386 cloud-free days
Costa et al. (2006)	DD	AFE_{SW}	-116.9	7/04/2000	Korea	SSA = 0.76
Zhou et al. (2005)	DD	AFE_{SW}	-80/-48	Monthly aerosol climatology	North Africa and Arabian Peninsula	Depending on surface albedo
Saha et al. (2008)	C-BB Mixed	AFE_{SW}	-97.6 -81.5	2005-2006	French Mediterranean	0.7 < SSA < 0.8
Valenzuela et al. (2012)	DD	AFE_{SW}	-70	2005-2010	Spain	

Table A1. Mean relative difference (RD) in the UV, VIS, NIR, and SW net fluxes if SSA = 0.90 and g = 0.75 are compared with different SSA and g scenarios for different SZA values.

SZA	RD_{UV} (%)	RD_{VIS} (%)	RD_{NIR} (%)	RD_{SW} (%)
30	±3.4	±1.9	±0.9	±1.5
60	±4.9	±3.0	±1.5	±2.4

871 Figure Captions

872 **Figure 1.** Annual cycle of daily values of AOD at 440 nm by box whisker plots. Triangles and

873 horizontal solid lines indicate the monthly average and median values, respectively.

874 **Figure 2.** Annual cycle of daily values of α ('alpha' in the figure) by box whisker plots. Triangles

875 and horizontal solid lines indicate the monthly average and median values, respectively.

876 **Figure 3.** Relative frequency of aerosol type occurrence: maritime (MA), desert dust (DD),

877 continental clean (CC), and continental polluted (CP).

878 **Figure 4.** Yearly values of AOD_{440nm} at the six sites: Barcelona (blue diamonds), Palencia (purple

879 triangles), Évora (red squares), Cabo da Roca (grey crosses), Granada (black stars), and El

880 Arenosillo (green circles). The text points out the statistically significant trend obtained.

881 **Figure 5.** Evolution of yearly ARE_{UV} (a), ARE_{VIS} (b), ARE_{NIR} (c), and ARE_{SW} (d) at the six sites:

882 Barcelona (blue diamonds), Palencia (purple triangles), Évora (red squares), Cabo da Roca (grey

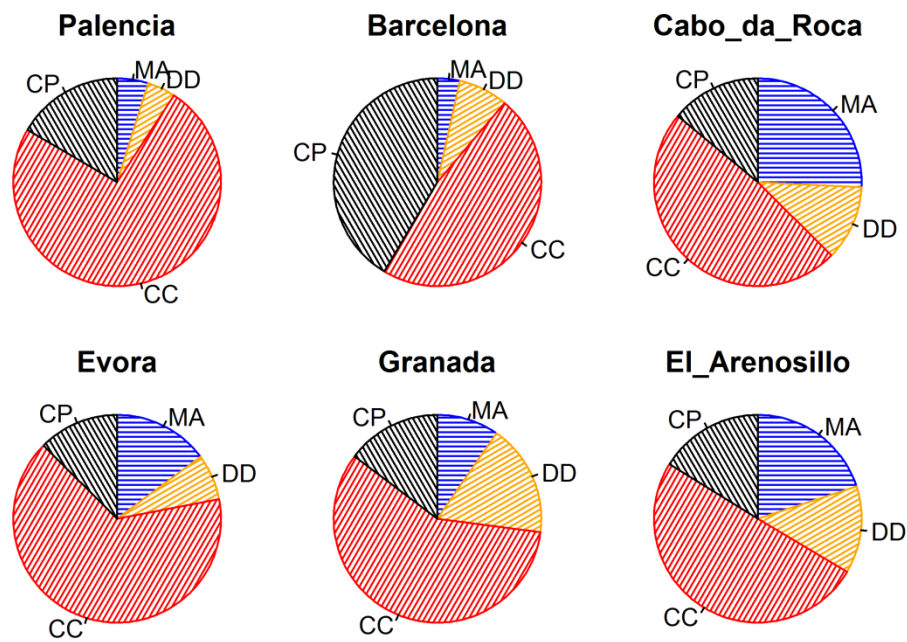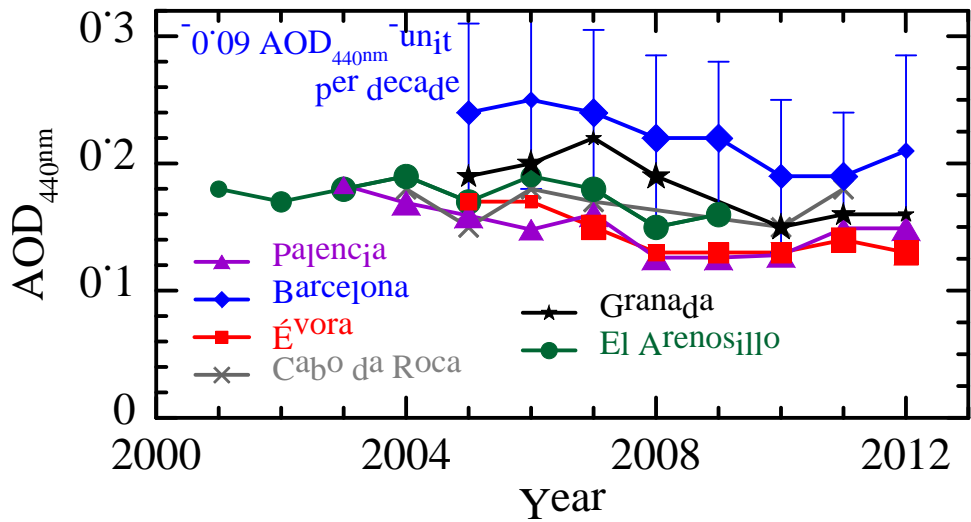883 crosses), Granada (black stars), and El Arenosillo (green circles). Vertical bars indicate the standard

884 deviation of each yearly value at Palencia station.

885 **Figure 6.** Evolution of annual ARE at the four spectral ranges (ARE_{UV} purple diamonds, ARE_{VIS}

886 red squares, ARE_{NIR} green triangles, and ARE_{SW} black circles) and AOD at 500 nm (blue stars)

887 averaging the data from the six Iberian ground-based sites (only years with at least three sites

888 considered). Dashed lines point out the linear trends (see text).

889 **Figure 7.** Annual cycle of ARE_{UV} (a), ARE_{VIS} (b), ARE_{NIR} (c), and ARE_{SW} (d) at the six sites:

890 Barcelona (blue diamonds), Palencia (purple triangles), Évora (red squares), Cabo da Roca (grey

891 crosses), Granada (black stars), and El Arenosillo (green circles). Vertical bars point out the

892 standard deviation of each monthly value at Évora station.

893   **Figure 8.** AFE_{UV}, AFE_{VIS}, AFE_{NIR}, and AFE_{SW} against four groups of aerosol single scattering

894   albedo and three intervals of α at the six sites: Barcelona (blue diamonds), Palencia (purple

895   triangles), Évora (red squares), Cabo da Roca (grey crosses), Granada (black stars), and El

896   Arenosillo (green circles).

897   **Figure 9.** Dependence of AFE_{VIS}/AFE_{SW} (a, c, e) and AFE_{NIR}/AFE_{SW} (b, d, f) ratios on SSA for

898   large (a, b), medium (c, d) and small (e, f) particles at the six sites: Barcelona (blue diamonds),

899   Palencia (purple triangles), Évora (red squares), Cabo da Roca (grey crosses), Granada (black stars),

900   and El Arenosillo (green circles).

901

902   Figure 1
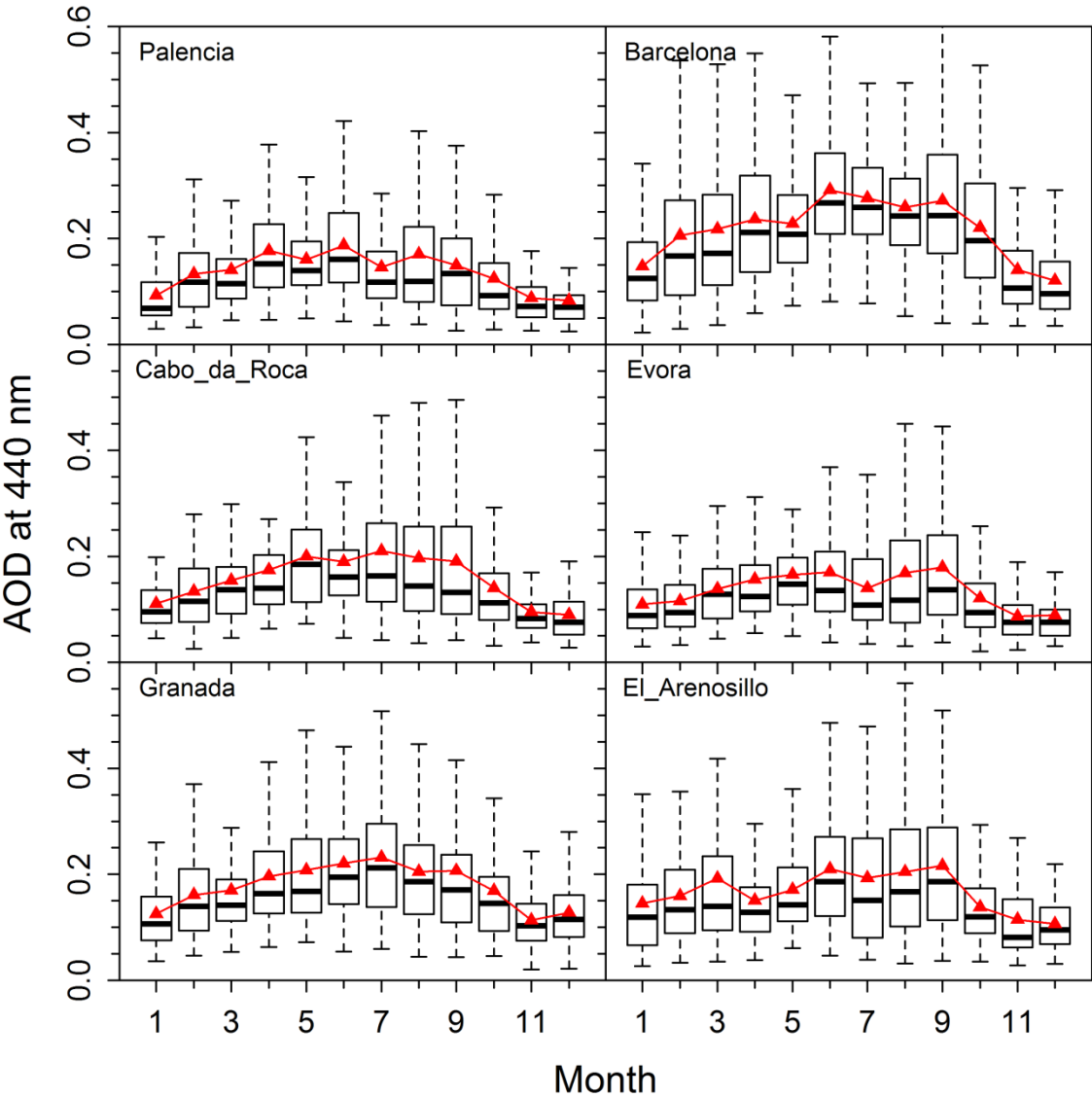
Figure 1. Annual cycle of daily values of AOD at 440 nm by box whisker plots. Triangles and horizontal solid lines indicate the monthly average and median values, respectively.

907   Figure 2
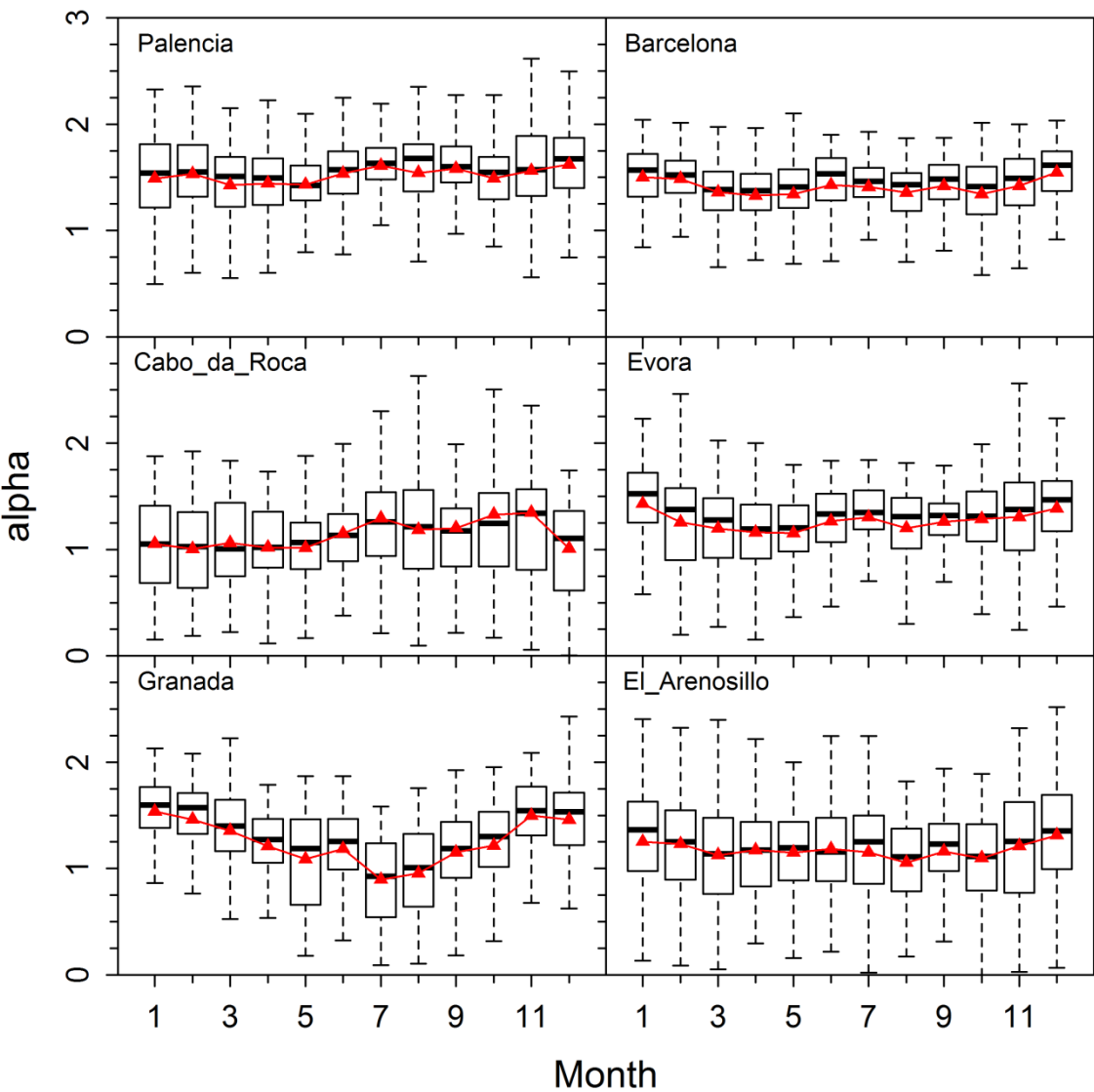
908

909   **Figure 2.** Annual cycle of daily values of α ('alpha' in the figure) by box whisker plots. Triangles

910   and horizontal solid lines indicate the monthly average and median values, respectively.

911

912

913   Figure 3

914

Figure 3. Relative frequency of aerosol type occurrence: maritime (MA), desert dust (DD), continental clean (CC), and continental polluted (CP).

Figure 4

Figure 4. Yearly values of AOD_{440nm} at the six sites: Barcelona (blue diamonds), Palencia (purple triangles), Évora (red squares), Cabo da Roca (grey crosses), Granada (black stars), and El Arenosillo (green circles). The text points out the statistically significant trend obtained. Vertical bars indicate the standard deviation of each yearly value at Barcelona station. Larger the symbols, large amount of data number that year (e.g., the smallest symbols indicate cases between 100 and 150 points, while the largest symbols show years with >250 points).

929   Figure 5
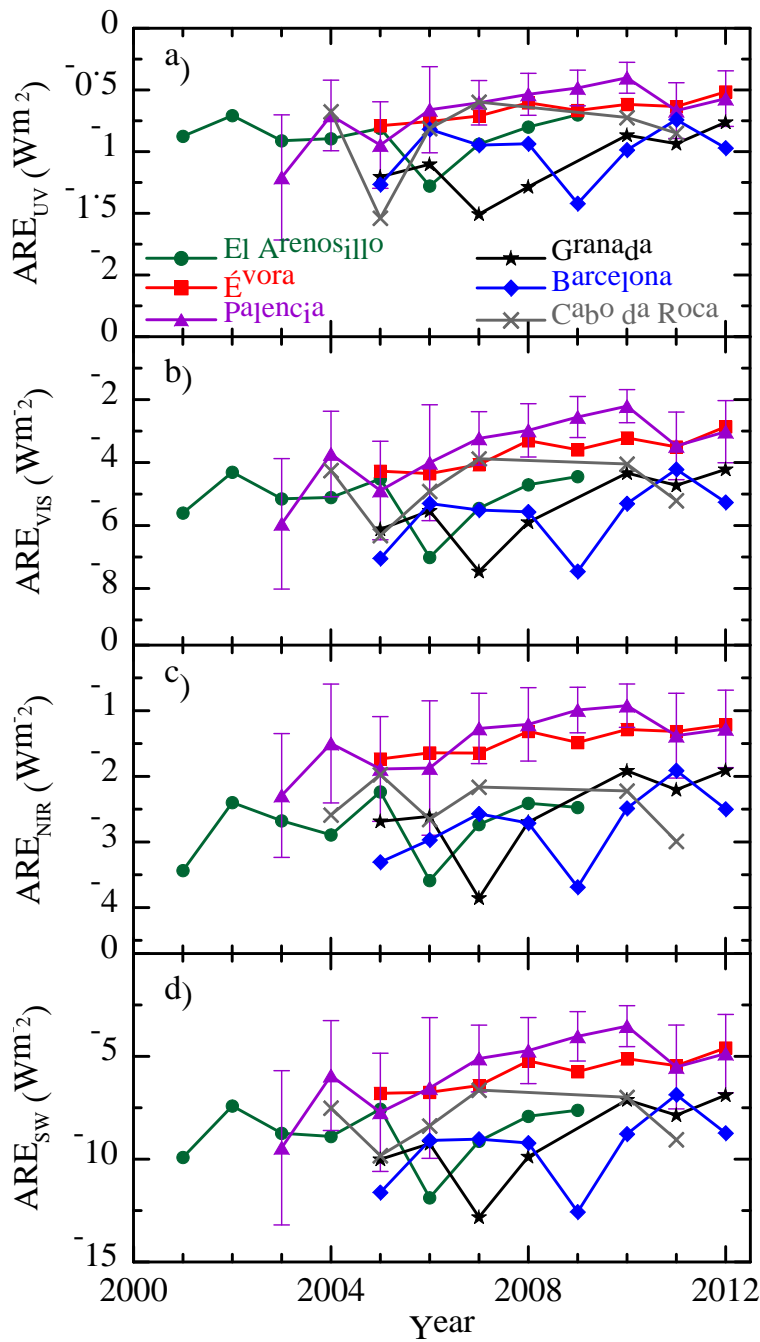
930

931   **Figure 5.** Evolution of yearly ARE_{UV} (a), ARE_{VIS} (b), ARE_{NIR} (c), and ARE_{SW} (d) at the six sites:

932   Barcelona (blue diamonds), Palencia (purple triangles), Évora (red squares), Cabo da Roca (grey

933   crosses), Granada (black stars), and El Arenosillo (green circles). Vertical bars indicate the standard

934   deviation of each yearly value at Palencia station.
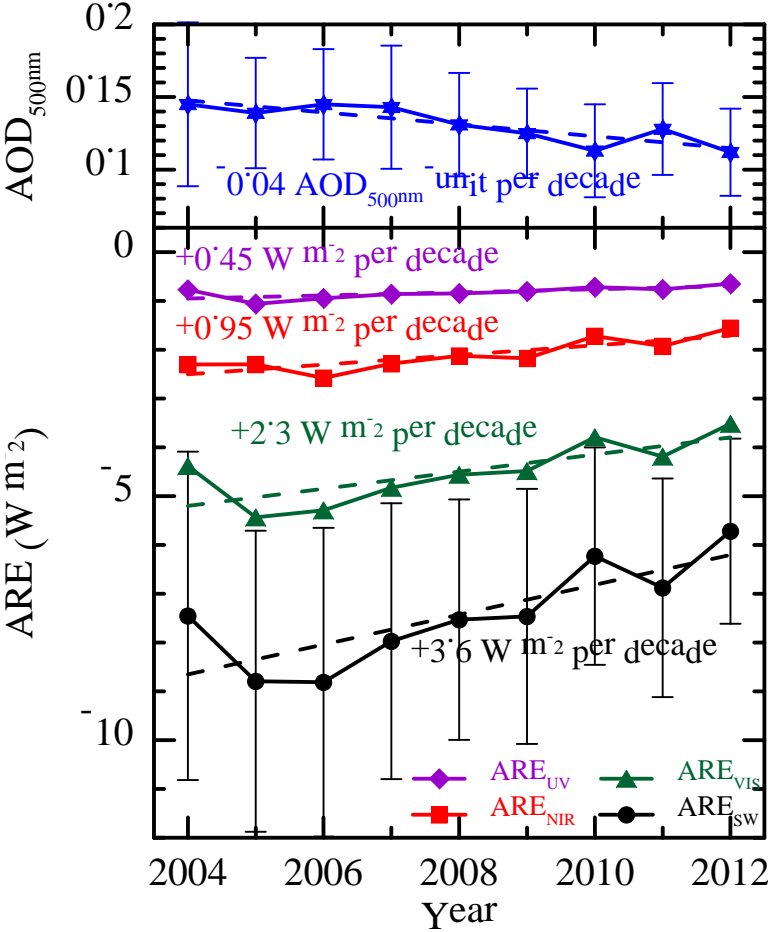
Figure 6. Evolution of annual ARE at the four spectral ranges (ARE_{UV} purple diamonds, ARE_{VIS} red squares, ARE_{NIR} green triangles, and ARE_{SW} black circles) and AOD at 500 nm (blue stars) averaging the data from the six Iberian ground-based sites (only years with, at least, three sites are considered). Dashed lines point out the linear trends (see text). Vertical bars indicate the standard deviation.
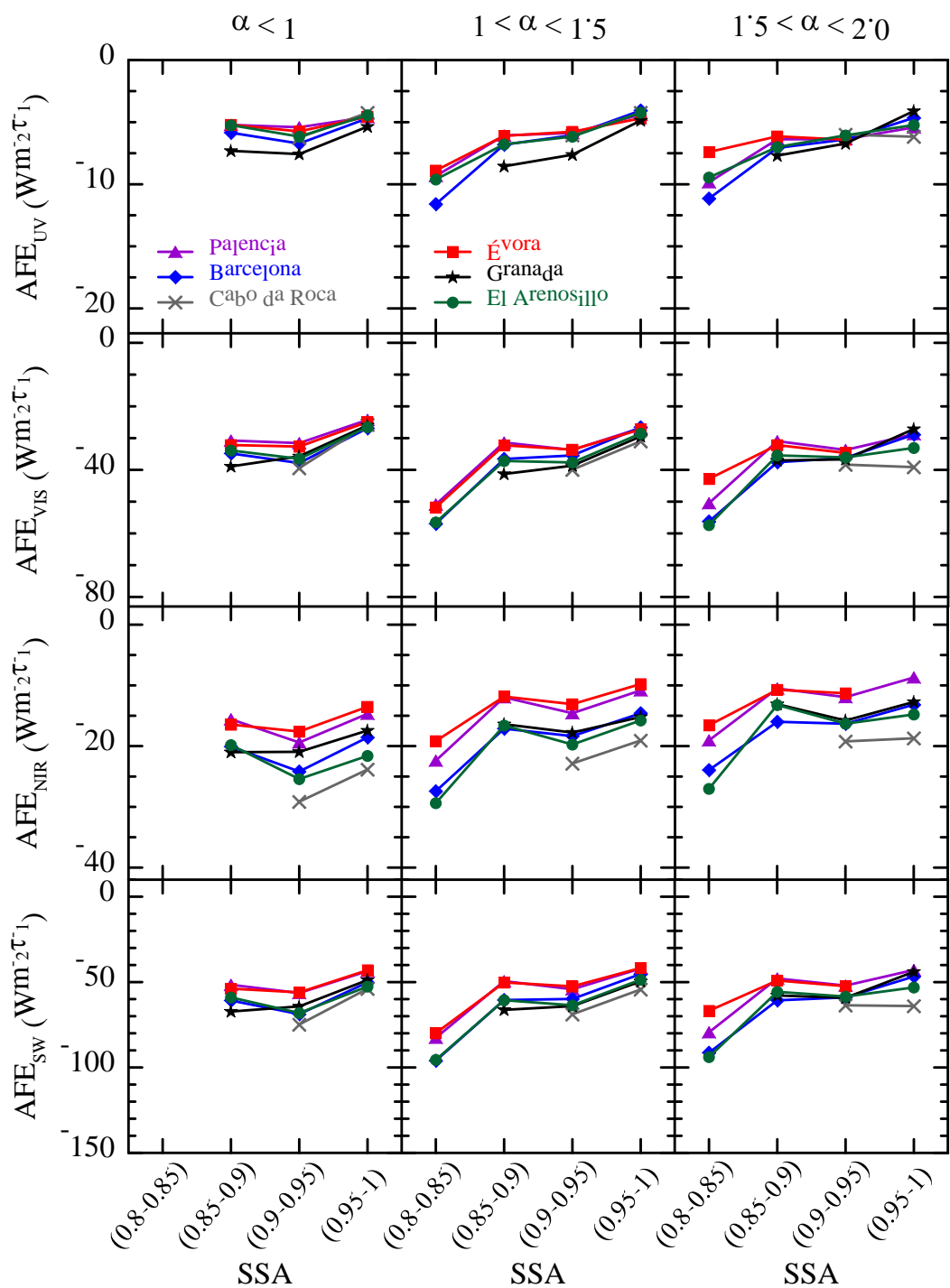
945

946   Figure 7
947
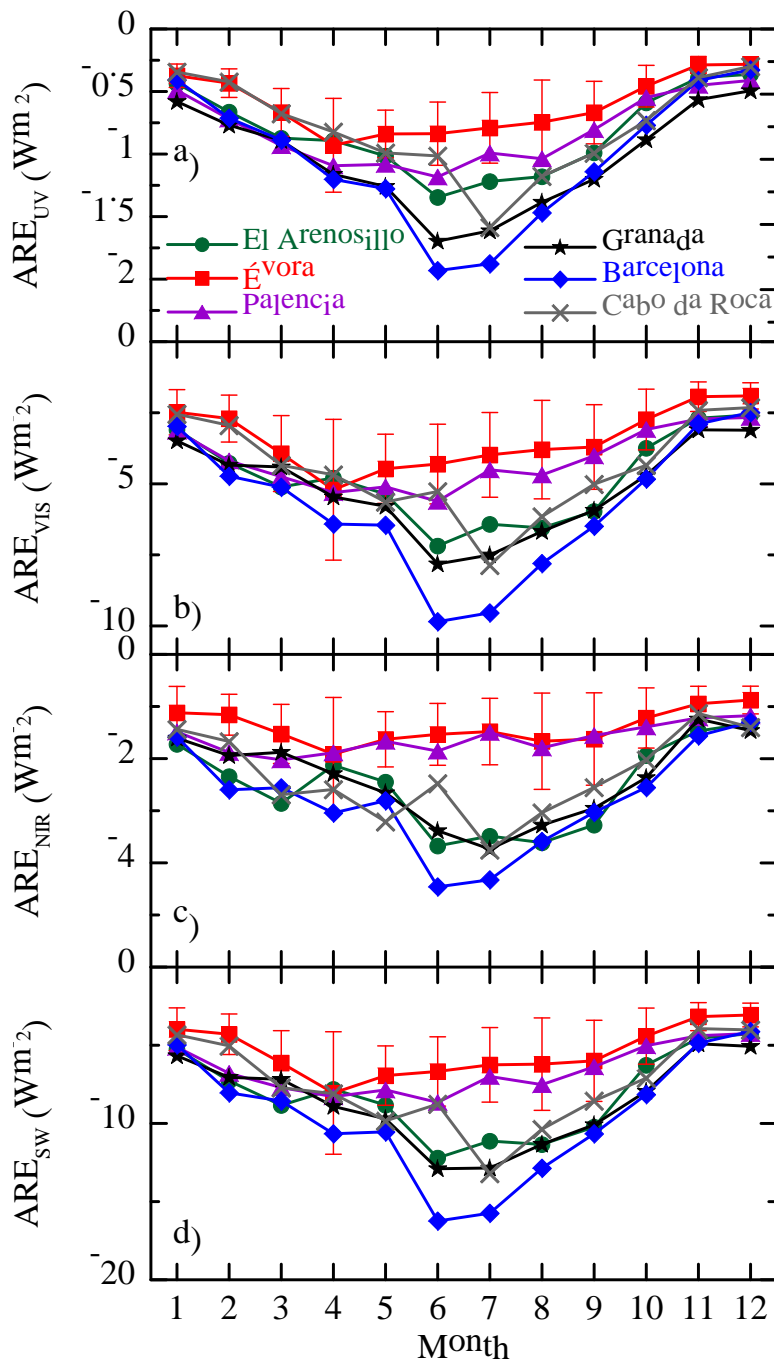
948

Figure 7. Annual cycle of ARE_{UV} (a), ARE_{VIS} (b), ARE_{NIR} (c), and ARE_{SW} (d) at the six sites:
Barcelona (blue diamonds), Palencia (purple triangles), Évora (red squares), Cabo da Roca (grey
crosses), Granada (black stars), and El Arenosillo (green circles). Vertical bars point out the
standard deviation of each monthly value at Évora station.

953 Figure 8

Figure 8. AFE$_{UV}$, AFE$_{VIS}$, AFE$_{NIR}$, and AFE$_{SW}$ against four groups of aerosol single scattering albedo and three intervals of α at the six sites: Barcelona (blue diamonds), Palencia (purple triangles), Évora (red squares), Cabo da Roca (grey crosses), Granada (black stars), and El Arenosillo (green circles).
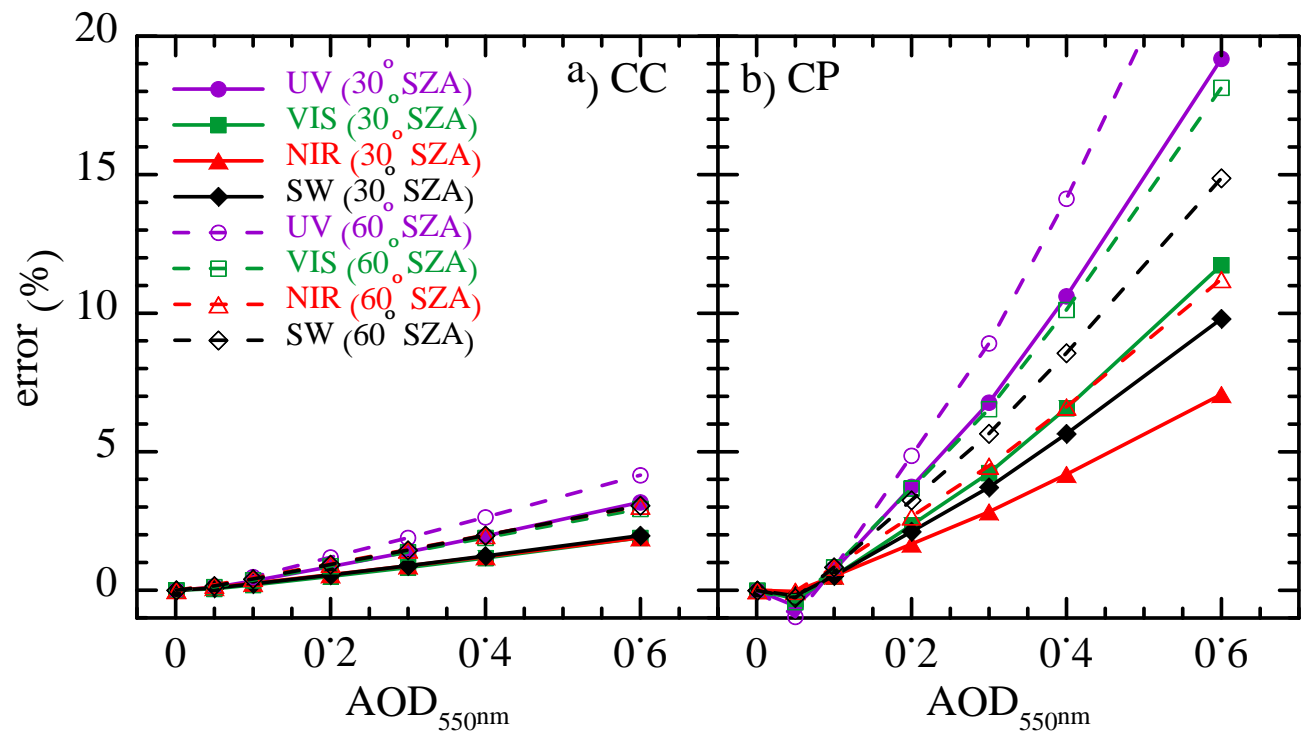
959 Figure 9

960
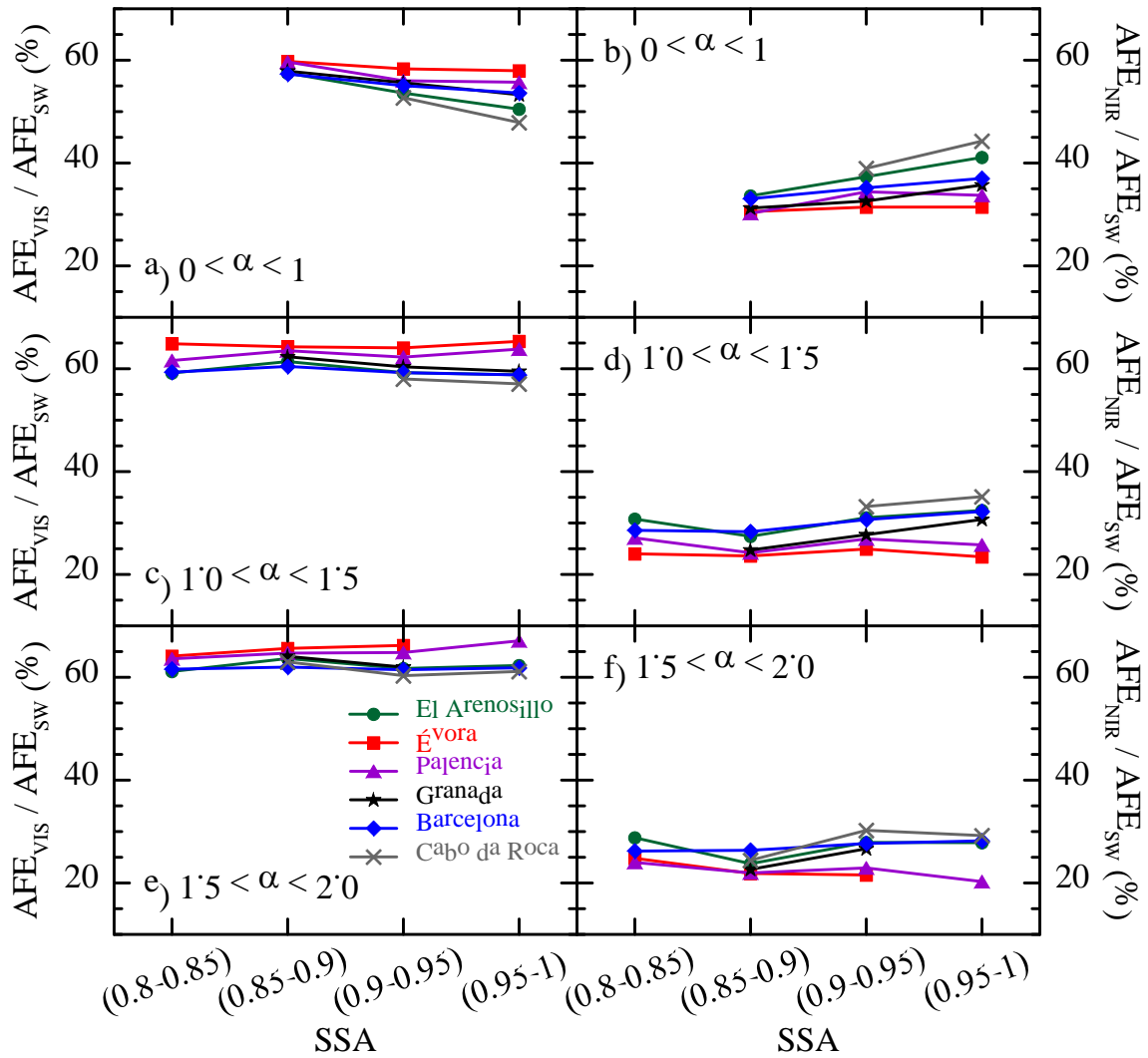
961

Figure 9. Dependence of AFE$_{VIS}$/AFE$_{SW}$ (a, c, e) and AFE$_{NIR}$/AFE$_{SW}$ (b, d, f) ratios on SSA for

large (a, b), medium (c, d) and small (e, f) particles at the six sites: Barcelona (blue diamonds),

Palencia (purple triangles), Évora (red squares), Cabo da Roca (grey crosses), Granada (black stars),

and El Arenosillo (green circles).

966

967 Figure A1

968

969

970 Figure A1. Dependence on aerosol load of the error committed when the optical properties are fixed

971 in the different spectral ranges for two SZAs (30º solid lines and symbols, and 60º dashed lines and

972 open symbols), and continental clean (CC, a) and continental polluted (CP, b) aerosols.

973